

Slip-rate estimate and past earthquakes on the Doruneh fault, eastern Iran

M. Fattahi,^{1,2*} R. T. Walker,³ M. M. Khatib,⁴ A. Dolati⁵ and A. Bahroudi⁵

¹The Institute of Geophysics, Tehran University, Kargar Shomali, Tehran, Iran

²School of Geography, Oxford Centre for the Environment, South Parks Road, Oxford OX1 3QY, UK

³Department of Earth Sciences, University of Oxford, Parks Road, Oxford, OX1 3PR, UK. E-mail: richw@earth.ox.ac.uk

⁴Department of Geology, Birjand University, Birjand, Iran

⁵Geological Survey of Iran, Azadi Sq., Meraj Avenue, PO Box 13185–1494, Tehran, Iran

Accepted 2006 September 27. Received 2006 August 10; in original form 2006 March 15

SUMMARY

The Doruneh fault, with a length of ~600 km, is one of the longest, and most prominent, faults in Iran. It performs an important role in the regional tectonics, but has no record of large earthquakes. The geomorphology of the Doruneh fault contains numerous indications of cumulative left-lateral slip over various scales. We describe three sites where Late Quaternary landforms are displaced by the fault. (a) An incised alluvial fan near the village of Uch Palang is displaced by 800–850 m. (b) The Kuh-e Teagh-Ahmad fold is composed of folded Quaternary gravels and is displaced by ~200–400 m. (c) A sequence of three terraces of the Shesh–Taraz river are displaced left-laterally by a maximum of 25 m. Infrared stimulated luminescence (IRSL) dating of the uppermost Shesh–Taraz river terrace gives a deposition age of ~10 ka, which correlates with changes in global climate ~10–12 ka ago, and provides a provisional slip-rate estimate of $2.4 \pm 0.3 \text{ mm yr}^{-1}$. No major recent or historical earthquakes are recorded on the Doruneh fault. Relatively fresh scarps and partially infilled fractures appear to be the preserved surface ruptures from an earthquake event of unknown age. A series of small streams showing left-lateral displacements of 3 to 5.5 m (with an average slip of ~4.7 m) record the possible magnitude of slip during this earthquake, which from scaling relationships would have had an M_w of ~7.5, and ruptured the fault over a length of >100 km. At the estimated slip-rate of ~2.5 mm yr⁻¹, the average recurrence time between large-magnitude earthquakes on the Doruneh fault is ~2000 yr.

Key words: Doruneh fault, earthquake hazard, Iran, slip-rate, strike-slip.

1 INTRODUCTION

The ~600 km long Doruneh left-lateral strike-slip fault was first described by Wellman (1966). It is one of the longest, and most clearly identifiable, active faults in Iran (e.g. Figs 1 and 2), and is likely to perform an important role in the regional tectonics, by accommodating up to 15 mm yr^{-1} of north–south right-lateral shear between central Iran and Afghanistan (Vernant *et al.* 2004). The accommodation of this strain is likely to involve a vertical axis clockwise rotation of the Doruneh fault (e.g. Jackson & McKenzie 1984; Jackson *et al.* 1995; Walker & Jackson 2004).

Despite the very clear expression of the Doruneh fault in the geomorphology, and its apparent major role in accommodating north–south right-lateral shear across eastern Iran, relatively few earthquakes have been recorded in the region (e.g. Ambraseys & Melville

1977). The low rate of seismicity on the Doruneh fault is in contrast to the neighbouring Dasht-e Bayaz region, which appears to play a similar role in the regional tectonics (e.g. Walker *et al.* 2004), but which has suffered from many earthquakes recorded both instrumentally and historically (e.g. Berberian & Yeats 1999, 2001; Walker *et al.* 2004). Determining whether the Doruneh fault is capable of generating large-magnitude earthquakes similar to (or larger than) the destructive events in the Dasht-e Bayaz region is clearly of prime importance for estimating the risk the fault poses to local populations. The Doruneh fault bounds large stretches of fertile and relatively densely populated farming land. The fault is also at least 600 km long, stretching from the Afghan border in eastern Iran, to the deserts of central Iran (e.g. Fig. 1). From scaling relationships (e.g. Scholz 1982; Wells & Coppersmith 1994) faults such as the Doruneh fault with lengths >100 km have the potential to produce earthquakes with magnitudes of >7.5.

We first summarize the role of the Doruneh fault in the active tectonics of Iran, and describe the historical, and instrumental record of earthquakes in the region. We then report remote sensing and

*E-mail: morteza.fattahi@ouce.ox.ac.uk

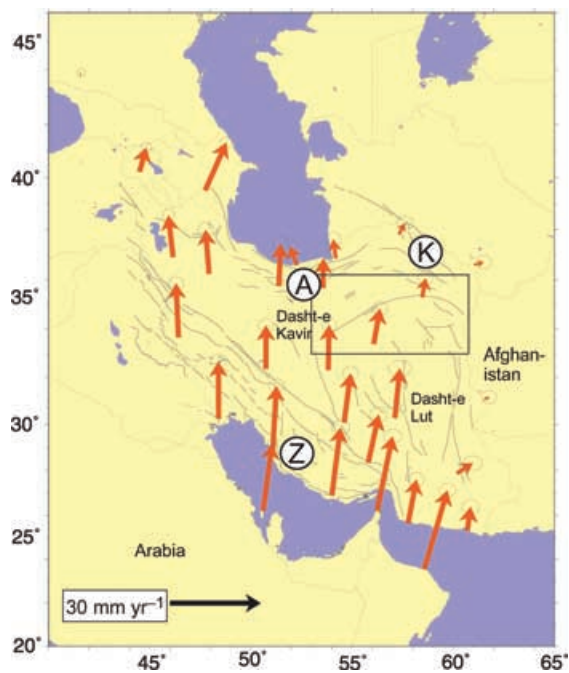


Figure 1. Map of Iran showing GPS velocities of points relative to Eurasia Vernant *et al.* (2004, from). The GPS velocities decrease to zero at both the northern and eastern margins of the country, suggesting that the Arabia-Eurasia convergence is accommodated within the borders of Iran. Most of the active deformation occurs in the seismically active Zagros (Z), Alborz (A) and Koppeh Dagh (K) mountain belts. 15 mm yr⁻¹ of north-south right-lateral shear is taken up across eastern Iran. North of latitude ~34°N, this right-lateral shear is accommodated on the east-west left-lateral Doruneh and Dasht-e Bayaz faults, which are thought to rotate clockwise about a vertical axis (e.g. Jackson & McKenzie 1984). Faults are from Berberian & Yeats (1999). The box shows the region represented in Fig. 2. This map is in a Mercator projection.

field evidence of cumulative left-lateral displacements at three main sites along the central part of the Doruneh fault close to the town of Kashmar. Luminescence dating of sediments, and inferred ages of the landforms from correlation with late Quaternary changes in climate, are used to determine a preliminary estimate of left-lateral slip-rate of ~2.5 mm yr⁻¹. Potential remnants of a large magnitude earthquake of unknown age are identified in the field.

2 ACTIVE TECTONICS AND SEISMICITY IN THE DORUNEH REGION

2.1 Active tectonics of Iran

The active tectonics of Iran are controlled by the northward motion of Arabia with respect to Eurasia, which has a velocity of ~25 mm yr⁻¹ at longitude 56°E (Fig. 1; Vernant *et al.* 2004). Continental shortening is broadly confined to within the political borders of Iran. Surrounding parts of Turkmenistan, Afghanistan and Pakistan appear to behave as non-deforming parts of stable Eurasia. Shortening within Iran is accommodated in the seismically active Zagros mountains in the south of the country and the Alborz-Koppeh Dagh ranges in the north (Fig. 1). The deforming regions are separated by the virtually aseismic, low-lying and extremely arid Dasht-e Kavir and Dasht-e Lut depressions of central Iran.

The central parts of Iran are moving northwards with respect to western Afghanistan at ~15 mm yr⁻¹ (Vernant *et al.* 2004). This northward motion introduces ~15 mm yr⁻¹ of north-south right-lateral shear across eastern Iran which is accommodated on right-lateral strike-slip fault systems on both the western (Gowk-Nayband fault system) and eastern (Neh and Zahedan fault systems) margins of the aseismic Dasht-e Lut desert (e.g. Walker & Jackson 2004; Regard *et al.* 2005). North of latitude ~34°N, deformation is accommodated on east-west left-lateral faults, including the Dasht-e Bayaz and Doruneh faults, which must rotate clockwise about a

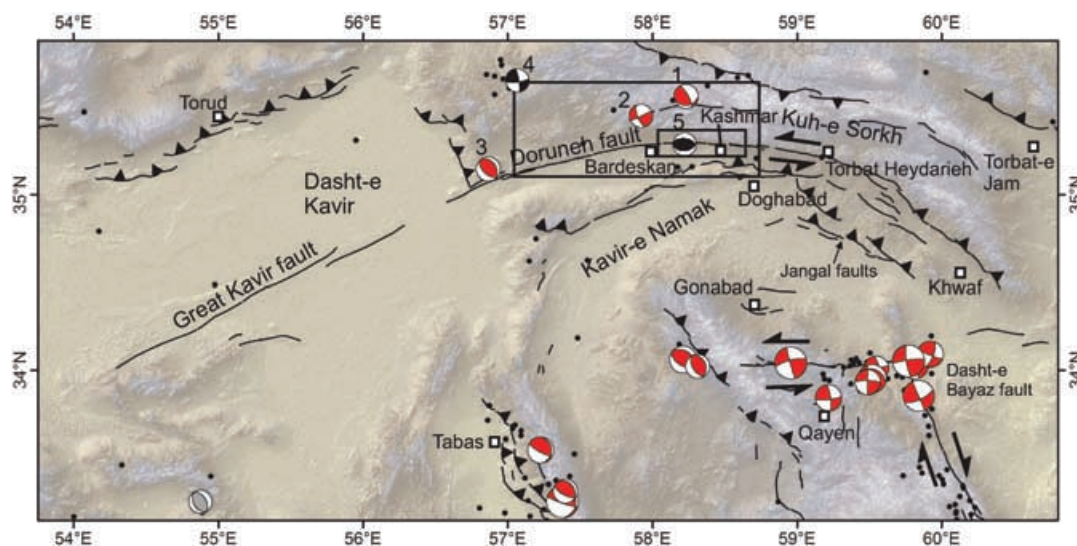


Figure 2. Map of the Doruneh fault with fault-plane solutions of recent earthquakes. Solutions determined by body-waveform modelling are shown in red. Harvard CMT solutions are black. The single first motion solution is in grey (from McKenzie (1972)) The source parameters of the five numbered solutions are given in Table 1. Black dots represent the epicentres of earthquakes up to 2004 from an updated version of the catalogue of Engdahl *et al.* (1998). Destructive historical earthquakes are known from Khwaf (1336 AD), from Doghabad (1619 AD), from Kashmar (the Turshiz earthquake, 1903.09.25), and from Torbat Heydarieh (1923.05.25). See Ambraseys & Melville (1982) and Section 2.2 for further details of these historic events. The small box represents the location of Fig. 3, and the large box shows the location of Fig. 11. This map is in a Mercator projection.

vertical axis if they are to accommodate the north–south right-lateral shear shown by GPS (e.g. Jackson & McKenzie 1984; Jackson *et al.* 1995; Walker & Jackson 2004; Allen *et al.* 2006). Walker & Jackson (2004) estimate a left-lateral slip-rate of 2.5–10 mm yr⁻¹ on the Doruneh fault assuming that the left-lateral slip arises from rigid block rotations. However, the model of Walker & Jackson (2004) is a simplification of the actual kinematics, as some diffuse deformation must occur within the fault-bounded blocks. A minimum slip-rate of 2.5 mm yr⁻¹ is estimated on the Dasht-e Bayaz fault to the south from the offset of ancient man-made features (Berberian & Yeats 1999).

2.2 Seismicity in the Doruneh region

The earliest recorded event in the Doruneh region is the 1336 AD Khwaf earthquake, which occurred early in the morning of the 21st October, and caused destruction over a wide area in the region south-east of Torbat-e Heydarieh and east of Khwaf (e.g. Ambraseys & Melville 1977, see Fig. 2). The meizoseismal area was ~110 km long and oriented roughly NW–SE (Ambraseys & Melville 1982). Given the location and orientation of the damage zone, the earthquake is likely to have ruptured thrust faults within the Jangal thrust fault system, which runs parallel, and to the south of, the Kuh-e Sorkh range-front and Doruneh fault (Fig. 2). In 1619 May AD, the village

of Doghbad (Dughabad) was destroyed, with ~800 deaths, by a substantial earthquake (Ambraseys & Melville 1982). The Dughabad earthquake happened during the daytime when most of the people were working in the fields otherwise the death toll is likely to have been higher. Although we have no information on the regional extent of damage, the reports suggest it was a reasonably large magnitude event (Ambraseys & Melville 1982). Given that Doghbad is situated south of the main Doruneh fault, and is close to a series of east–west thrust faults, it is likely that this earthquake involved slip on these thrust faults.

The 25th September 1903 Turshiz earthquake is described by Ambraseys & Moinfar (1975) and Ambraseys & Melville (1982). The earthquake caused extensive damage in an east–west region extending ~40 km west from Kashmar (then known as Turshiz) to the village of Kishmar (Fig. 3). The southern parts of Kashmar were almost totally destroyed and the northern suburbs damaged. Outlying settlements west of Kashmar were totally destroyed. Roughly 350 people were killed in total. Thirteenth century minarets at Kishmar (Fig. 3) and Firuzabad (~20 km southwest of Kishmar) were not damaged by the earthquake. Although the distribution of damage is parallel to the Doruneh fault trace, the meizoseismal zone is not centred on the Doruneh fault. All reports of damage are for villages close to, but south of, the Doruneh fault, and there are no records of damage to isolated villages north of the Doruneh fault. This uneven

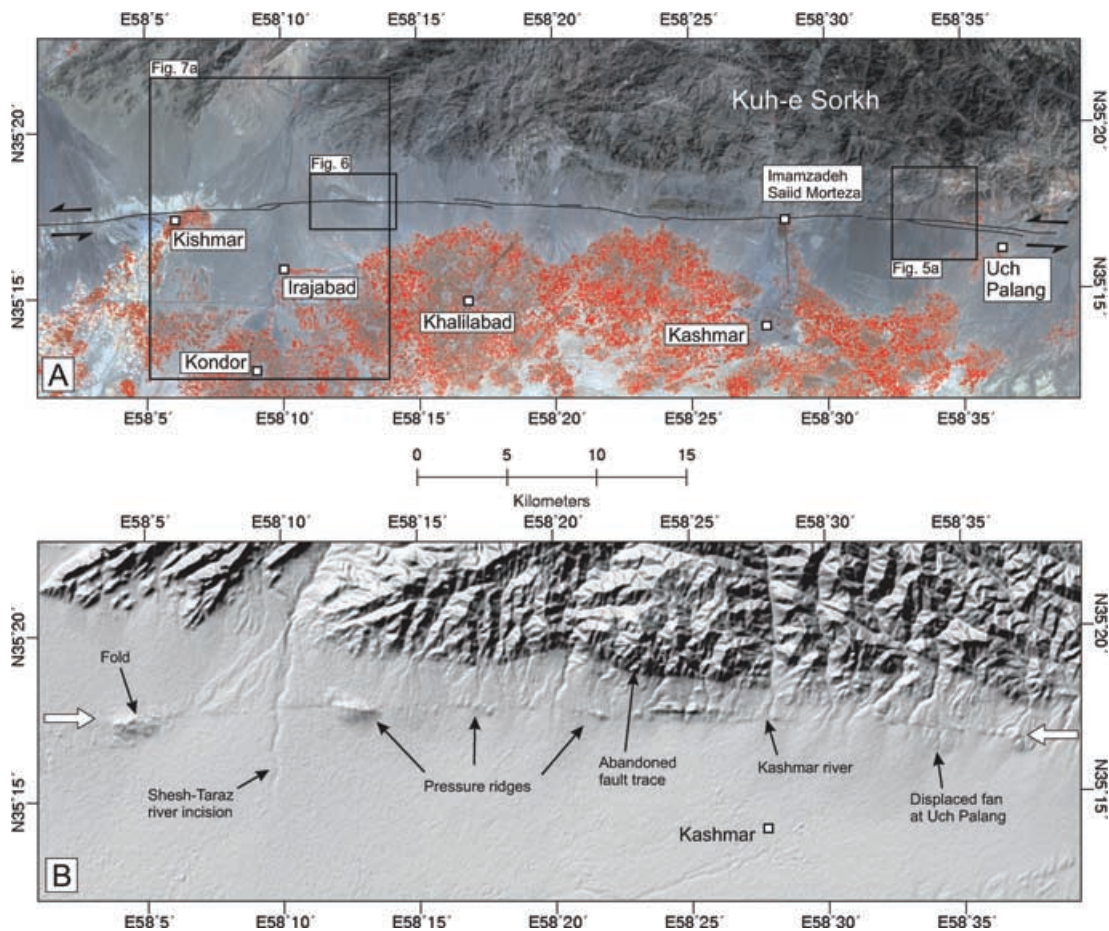


Figure 3. (a) ASTER satellite image (RGB 321 with 15 m pixel spacing) of the central Doruneh fault near Kashmar (see Fig. 2 for location). The fault runs east–west across the centre of the image, separating bedrock exposure of Kuh-e Sorkh in the north, from vegetated farmland in the south (vegetation is red in this image). (b) SRTM digital topography illuminated from the northwest of the same region as in Fig. 3(a). The incision of the Shesh–Taraz river is visible. Details of the fault trace (running between the white arrows) are also visible, with clear south-facing scarps and short pressure ridges formed at right-stepping bends in the fault. This, and all later maps, are in a UTM-40 projection.

Table 1. Epicentres and source parameters of earthquakes in the Doruneh region. Events 1 to 3 are from Baker (1993), and are also listed in Jackson (2001). Events 4 and 5 are from the Harvard CMT catalogue (<http://www.seismology.harvard.edu/CMTsearch.html>). Depths reported for the CMT events are not necessarily reliable (e.g. Jackson 2001).

Event	Date	Time (GMT)	Latitude	Longitude	Depth	M_w	Strike	Dip	Rake
1	1971.05.26	02:41:35	35.56	58.23	13	5.6	89	26	32
2	1972.12.01	11:39:35	35.45	57.92	8	5.3	65	87	25
3	1979.12.09	09:12:35	35.15	56.87	9	5.5	325	36	99
4	1996.02.25	17:42:04	35.65	57.07	33	5.4	82	77	10
5	2000.02.02	22:58:01	35.29	58.22	26	5.3	83	43	79

distribution may be due to local site effects, with greater levels of damage in those villages sited on unconsolidated alluvium south of the fault, and lesser damage to those villages sited on bedrock. However, the earthquake might have instead occurred on a fault immediately south of the Doruneh fault (Ambraseys & Melville 1982). Northward-dipping east–west thrust faults are present south of Kashmar (Fig. 2). It is therefore possible that the 1903 earthquake happened on deep parts of these thrust faults rather than on the main Doruneh fault.

The most recent destructive earthquake to have occurred in the Doruneh region is the 1923 May 25th Kaj-Darakht event (Ambraseys & Moinfar 1977). This earthquake resulted in the destruction of five villages (within an area of radius ~ 5 km), and caused serious damage to a further twenty, leaving ~ 770 casualties (Ambraseys & Melville 1982). The major damage occurred in an ~ 20 km long region, directly southwest of Torbat Heydarieh. From the damage distribution it is likely that the earthquake occurred on the Doruneh fault. The relatively small epicentral zone, and the absence of surface rupturing, suggests a reasonably small magnitude (estimated at M_s 5.8 by Ambraseys & Moinfar 1977).

Fault-plane solutions of instrumental seismicity are shown in Fig. 2. Source parameters and epicentres of the five earthquakes from the Doruneh region are also included in Table 1. Source parameters of the Tabas and Dasht-e Bayaz earthquake sequences (in the south of Fig. 2) are provided in Walker *et al.* (2003) and Walker *et al.* (2004) and references therein. Only one of the five instrumentally recorded Doruneh events (2000.02.02, event five in Table 1) has an epicentre close to the Doruneh fault, with the other four presumably occurring on faults within Kuh-e Sorkh (Fig. 2). The epicentre of the M_w 5.3 2000.02.02 event is slightly south of the Doruneh fault, located between Kashmar and Bardeskan, and has a Harvard CMT solution showing almost pure thrusting. It therefore appears that this earthquake occurred on the north-dipping east–west thrusts which run parallel to the Doruneh fault, and which are also likely to have caused the destructive earthquakes in 1619 and 1903.

It is clear that, although destructive earthquakes have occurred in this part of northeast Iran, only the 1923 Kaj Darakht—and possibly the 1903 Turshiz earthquakes—are likely to have occurred on the Doruneh fault itself. The other recorded events are associated with active structures to the north and south of the main Doruneh trace. Both the 1903 and 1923 earthquakes are not likely to have been large magnitude events. One of the major aims of this paper is to investigate whether the apparent low level of seismicity on the Doruneh fault is real, or whether it has the potential to produce large magnitude earthquakes in future.

3 GEOMORPHOLOGY OF THE CENTRAL DORUNEH FAULT

The Doruneh fault is one of the longest fault systems in Iran, and stretches for ~ 600 km from the Afghan border in the east, to the

Dasht-e Kavir desert of central Iran (Figs 1 and 2). Clear scarps in alluvial fans and river terraces are seen along the entire fault length and can be observed both in satellite imagery and in the field. A section through the fault at Imamzadeh Saiid Morteza (a shrine directly north of Kashmar, see Fig. 3) exposes a steeply north-dipping fault plane (Fig. 4). The north-dipping fault exposure and southward-facing scarps at Imamzadeh Saiid Morteza indicate a slight component of shortening in that locality. The component of vertical displacement is however very small in comparison with the lateral component, as seen from the detailed descriptions below. Further east, widespread thrusting suggests an increase in the component of shortening (Fig. 2). In the following section we describe locations, observed both in satellite imagery and in the field, that show indications of long-term left-lateral slip on the fault.

3.1 Left-lateral displacement of the Uch Palang alluvial fan

One of the clearest indications of cumulative left-lateral slip is found ~ 7 km east of Kashmar near the village of Uch Palang (Fig. 3), where a heavily dissected alluvial fan is cut by two parallel strands of the

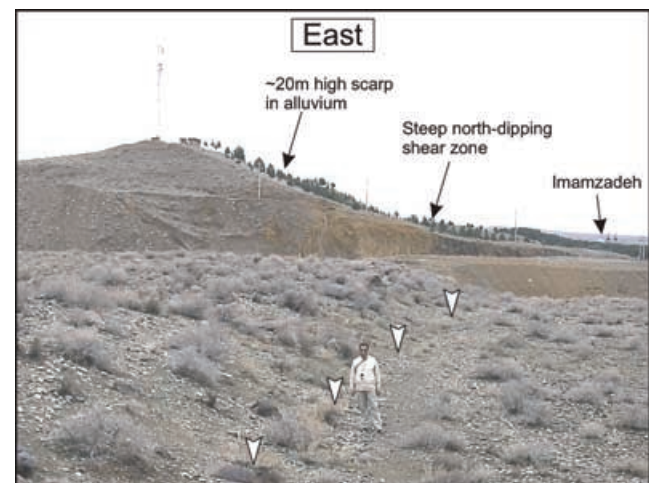


Figure 4. Field photograph looking across the Kashmar river, of a cross-section through the Doruneh fault at Imamzadeh Saiid Morteza, north of Kashmar (see Fig. 3a for location). The fault is ~ 100 m wide and contains numerous fault zones. The southernmost zone is the most recently active, separating light-coloured (to the north) from dark-coloured fault rocks, and outcrops at the base of an ~ 20 m high scarp in alluvium. The faults dip steeply northwards, and imply a slight component of reverse slip. In the foreground, the fault has formed a south-facing scarp, estimated in the field at ~ 1.5 – 2 m high, in river terrace material. The base of the scarp is marked by white arrows. The fault exposure is relatively new (compare with fig. 3 in Tchalenko *et al.* 1973).

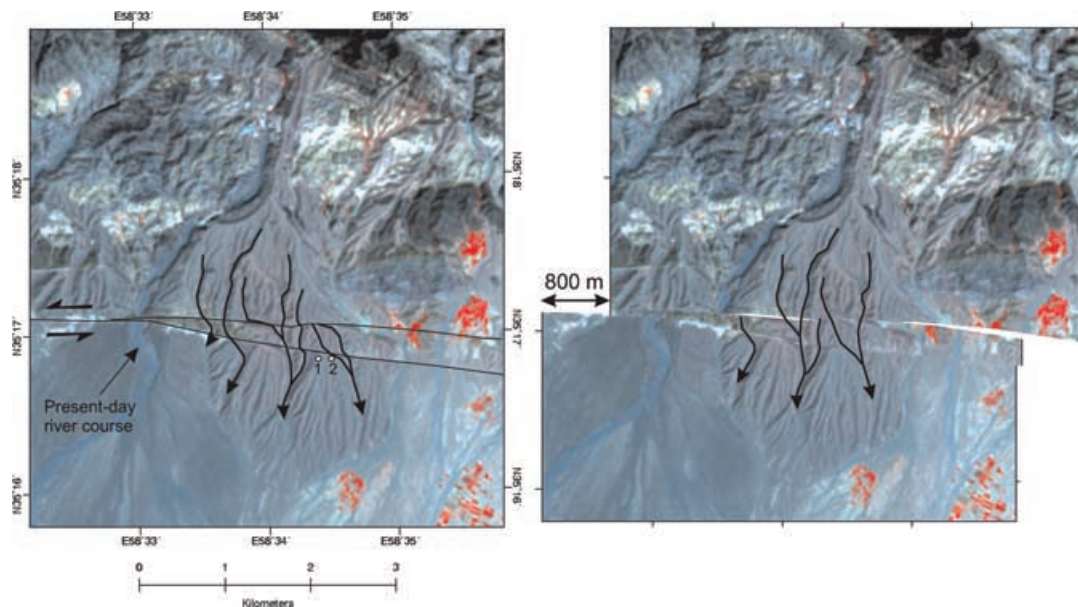


Figure 5. (a) ASTER satellite image (RGB 321) of an incised alluvial fan near the village of Uch Palang east of Kashmar (see Fig. 3 for location). The present-day course of the river follows the western margin of the fan. Two parallel strands of the Doruneh fault cut across the centre of the image. Both the fan itself, and streams incised into its surface, are apparently displaced left-laterally across the fault. The two numbered dots represent the OSL sampling locations Kfan1 and Kfan2 (see Appendix A). (b) Restoration of 800–850 m of left-lateral slip aligns both the incised drainage systems and the margins of the alluvial fan.

Doruneh fault (Fig. 5a). The present-day course of the river follows the western margin of the fan. Both the fan itself, and streams incised into its surface, appear to be displaced left-laterally across the fault. Restoration of 800–850 m of left-lateral slip aligns both the incised drainage systems and the margins of the alluvial fan (Fig. 5b).

The apparent left-lateral displacement of drainage incised into the Uch Palang fan was noted by Wellman (1966) and Giessner *et al.* (1984), who both use this area as an example of long-term left-lateral slip on the Doruneh fault. However, Tchalenko *et al.* (1973) interpret the stream deflections as being controlled by local topographic variations. From Fig. 5, we see that the drainage is deflected in a left-lateral sense on both the eastern and western margins of the fan. If the deflections were caused by the local topography, the streams would flow away from the apex of the fan, thus creating apparent left-lateral displacements on the eastern margin of the fan, and apparent right-lateral displacements on the western fan margin. The realignment of both the fan itself, and the consequent drainage on the fan surface, show that the reconstruction of 800–850 m of left-lateral slip is reliable.

3.2 Left-lateral displacement of Kuh-e Teagh Ahmad

Kuh-e Teagh-Ahmad is a small hill composed of Plio-Quaternary alluvial gravels (Taheri & Shamanian 2001). The gravels have been folded into a steep anticline, and underlying sandstones and marls are exposed in the core (e.g. Fig. 6). The Doruneh fault cuts through the centre of Kuh-e Teagh-Ahmad and displaces the western margin of the fold by ~ 200 m, and the eastern edge by ~ 400 m. There has therefore been at least 200–400 m of left-lateral slip on the Doruneh fault since the Teagh-Ahmad fold was abandoned. As both margins of the fold are susceptible to fluvial erosion by southward-flowing streams (Fig. 6), the true amount of slip might be higher.

3.3 Left-lateral displacement of the Shesh–Taraz river terraces

The Shesh–Taraz river originates in the Kuh-e Sorkh mountains and flows southwards to drain into the Kavir-e Namak basin (Fig. 2). The river is one of the largest regional drainage systems. It has incised through a large alluvial fan, leaving a series of river terraces (Fig. 7). Four main levels, including the top surface of the incised alluvial fan (T1), two paired erosional terraces (T2 and T3), and the active river channel are observed (Fig. 7; Giessner *et al.* 1984). Further minor, and often unpaired, terraces are present along parts of the river system (for instance T1a). Each of the major river terraces correlates southward with the deposition of an alluvial fan. The fan deposition appears to have migrated southward through time. The T1 fan surface is itself deposited on an older generation of alluvial fan (Fig. 7). A small vertical component on the Doruneh fault has generated steep southward-facing scarps in these older fan deposits.

The Doruneh fault cuts across the Shesh–Taraz river terraces, laterally displacing the terrace risers, and enabling us to determine the amount of slip since abandonment of the successive terraces (e.g. Van Der Woerd *et al.* 2002). The lateral displacement is clearest on the eastern bank of the river (Fig. 7c). Widening of the fault zone, and vertical fault movements within a small pull-apart basin, make restoration of the terrace risers extremely difficult on the western river bank (Fig. 7c). All three of the major terraces, as well as a minor channel bank on the T1 surface (T1a), are present where the fault cuts through the eastern bank of the river (Fig. 7c).

Fig. 8(a) shows a digital elevation model (DEM) of the terraces on the eastern river bank. The DEM was produced from differential GPS measurements. Contours are drawn at 2 m intervals and highlight the locations of the low relief terraces and the steep risers between them. The risers are marked by grey bars in Fig. 8(a). The exact edges of the terraces are difficult to see in plan view. We have therefore drawn parallel east–west profiles through the DEM on the northern and southern sides of the fault. The profiles are shown in

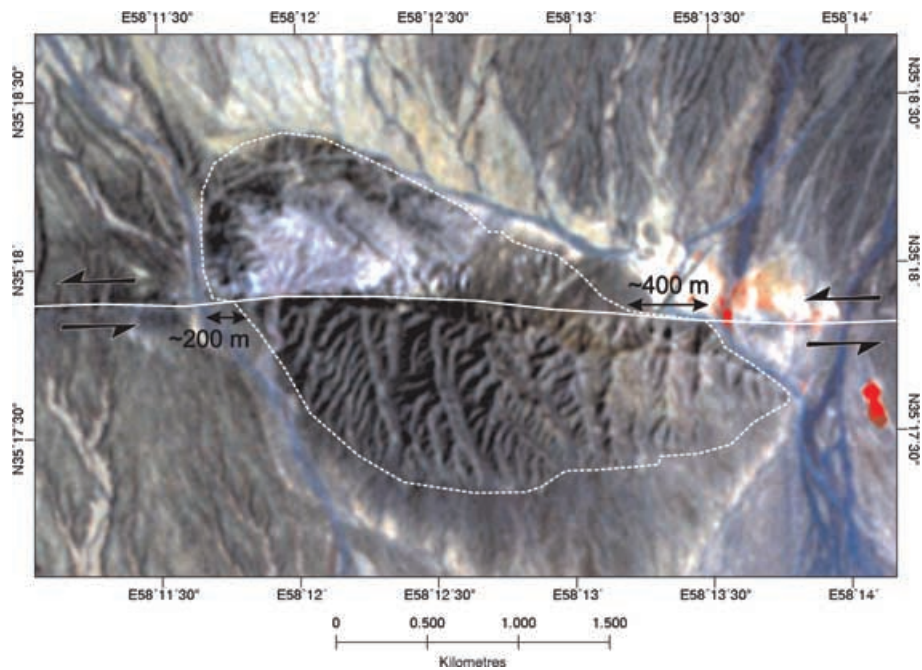


Figure 6. (a) ASTER satellite image (RGB 321) of Kuh-e Teagh Ahmad west of Kashmir (see Fig. 3 for location). The Doruneh fault cuts through the fold, and appears to displace the margins left-laterally by 200–400 m. Erosion of the fold flanks by southward flowing rivers may have hidden some of the displacement.

Fig. 8(b) and show that the apex of the T1a ridge is displaced by ~25 m across the fault and the edge of the T1 terrace is displaced by ~22 m (see also Fig. 9a). A stream incised into the T1 surface (at the right-hand side of Fig. 8a) is also displaced by ~25 m. Although the edge of T1 was susceptible to fluvial erosion whilst the Shesh–Taraz river was cutting T2, both the channel bank T1a, and the displaced stream cut into T1 were not susceptible to erosion at their edges. The 25 m of displacement of the T1a ridge is therefore likely to represent the total fault slip since abandonment of the T1 fan surface. The situation is less clear for the displacement of the lower terraces T2 and T3. The Doruneh fault has split into two strands (Fig. 8a) and our profiles only account for displacements across the northern trace. The T2 level is displaced laterally by at least 8 m. The vertical displacement across the T1 surface is very small in comparison to the 25 m of left-lateral slip (as seen in the profiles in Fig. 8b), and we do not consider dip-slip movement in our estimate of slip rate.

4 AGE OF THE DISPLACED LANDFORMS AND RATES OF LEFT-LATERAL SLIP ON THE DORUNEH FAULT

In the previous section we described the left-lateral displacement of geomorphic features by slip on the Doruneh fault. By determining the age of these features, we can use the offsets to determine the average rate of slip: information which is vital for investigating the role of the fault in the regional tectonics, and for estimates of the possible hazard from earthquakes. The only other information on slip-rate on the Doruneh fault is provided by Walker *et al.* (2004), who estimate between 2.5 and 10 mm yr⁻¹ of slip, based on a simple model of fault-bounded blocks rotating clockwise about a vertical axis (see Section 2.1).

We took six sediment samples—one from each of the Shesh–Taraz terraces, and two from the surface of the Irajabad alluvial fan—for age determination using infrared stimulated luminescence

dating (IRSL). An introduction to luminescence dating is given in Forman *et al.* (2000). Luminescence dating measures the time elapsed since last exposure to the sun of quartz and feldspar mineral grains within a sediment sample. Energy is stored within buried sediment grains due to ionizing radiation from the decay of radioactive isotopes of Th, U, ⁴⁰K and from cosmic rays. Laboratory illumination of the mineral grains by visible light or infrared energy releases the stored energy as luminescence. The level of observed luminescence is dependent on the absorbed radiation dose. For age determination two values are therefore required: the equivalent dose D_e (which is the total radiation level responsible for producing the luminescence signal), and the dose received per year (during burial).

In order to determine the age of deposition of a sediment sample, the mineral grains must have been exposed to sunlight when they were laid down. Exposure to sunlight releases any stored energy from earlier burial periods and thus resets the luminescence ‘clock’. Luminescence dating is therefore usually applied to fine-grained, low-energy deposits, in which the assumption of long exposure to sunlight is likely to be valid. However, the sediments in our study area are typically composed of relatively coarse alluvium. The real age of these coarse-grained deposits may be younger than the measured luminescence age as the high-energy alluvial deposition might not have permitted sufficient exposure to sunlight to fully reset the signal.

The reliability of calculated ages from coarse-grained deposits can be assessed using dose distribution diagrams, which are shown for our six samples in the appendix (Fig. A6). The dose distribution diagrams show the equivalent dose (D_e) measurements for experiments on multiple small subsamples (aliquots) of each specimen using the single aliquot regeneration method (e.g. Fattahi & Walker 2006). If the sediment is only partially reset, we would expect a large spread of measured D_e between individual aliquots, as each mineral grain within the sediment will have experienced a different storage and transport history prior to burial. If the sample was fully reset on deposition we would see close agreement in the measured

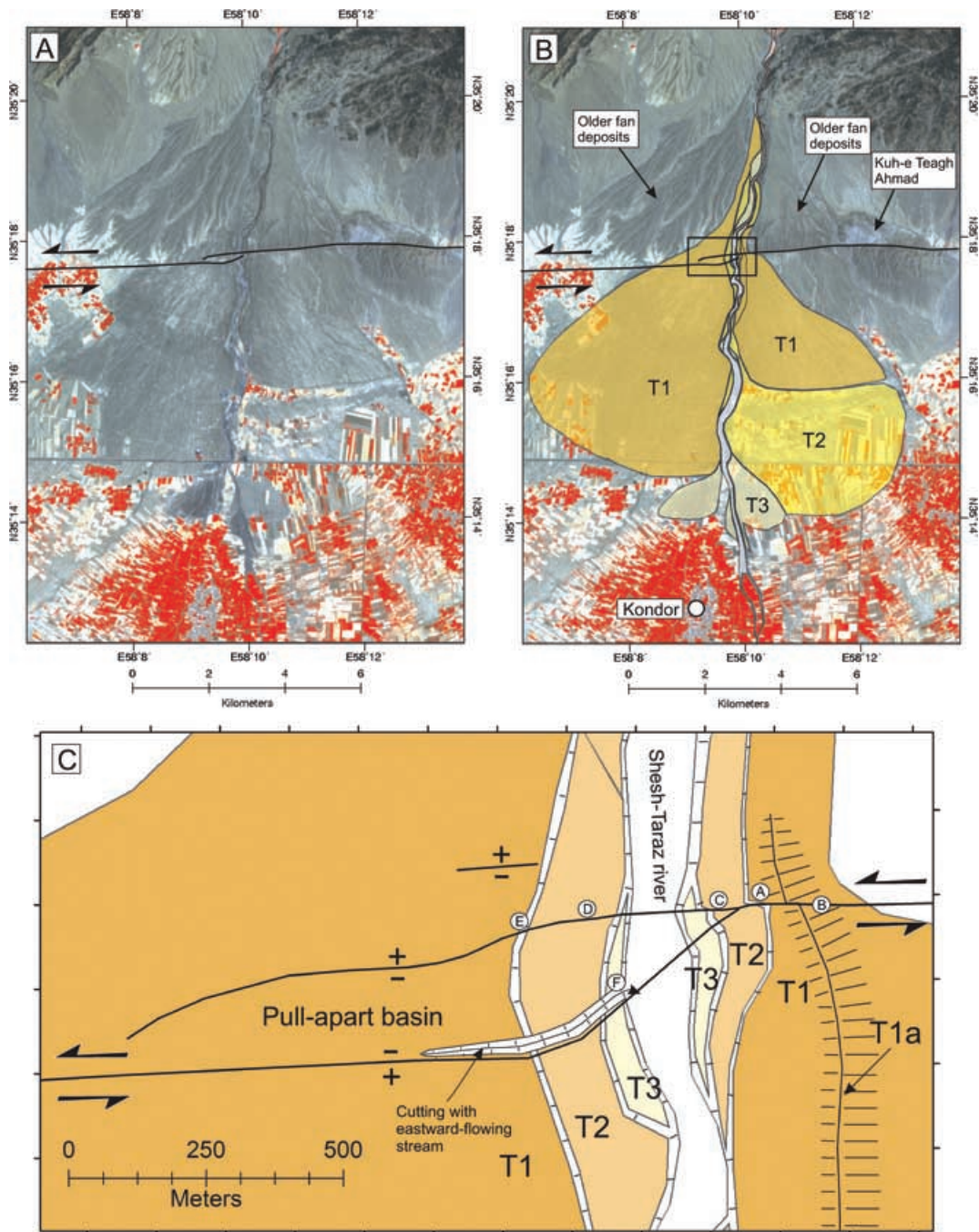


Figure 7. (a) ASTER satellite image (RGB 321) of the Shesh–Taraz river west of Kashmar (see Fig. 3 for location). The Doruneh fault cuts across the centre of the image and forms a small pull-apart basin where it crosses the river. (b) The same image overlain with the distribution of the three youngest periods of alluvial fan and river terrace deposition (mapped from satellite imagery, with reference to the map of Giessner *et al.* (1984)). The regionally extensive fan surface (T1) is incised by two major river terrace levels (T2 and T3), which each grade southwards into small alluvial fans. The sequence of terraces define a basinward migration of alluvial deposition through time. Remnants of older alluvial fans are present to both the east and west of the T1 fan. (c) Geomorphic map of the Shesh–Taraz river terraces where they are cut by the Doruneh fault (from Giessner *et al.* (1984) and our own observations), see box in Fig. 7b for location. Terraces on the eastern river bank show clear offsets across the fault. The amounts of displacement are difficult to determine on the western river bank as the fault zone has widened. A linear ridge (T1a) on the T1 fan surface is interpreted as an old channel bank deposit. Circled letters (a to f) show the approximate locations of the photographs in Fig. 9.

D_e for each aliquot of a given sample. The diagrams show a reasonable clustering of equivalent dose measurements for samples T1 and T1a and so in the following discussions we assume they reflect the luminescence from a completely reset material. The reader should remember that the true deposition ages might be lower, and

hence the measured slip-rates should be considered as minimum values.

The six sampling locations are marked on Figs 5a and 8a. Samples for IRSL analysis are usually taken from uniformly fine-grained deposits, and are collected either by inserting a tube into soft

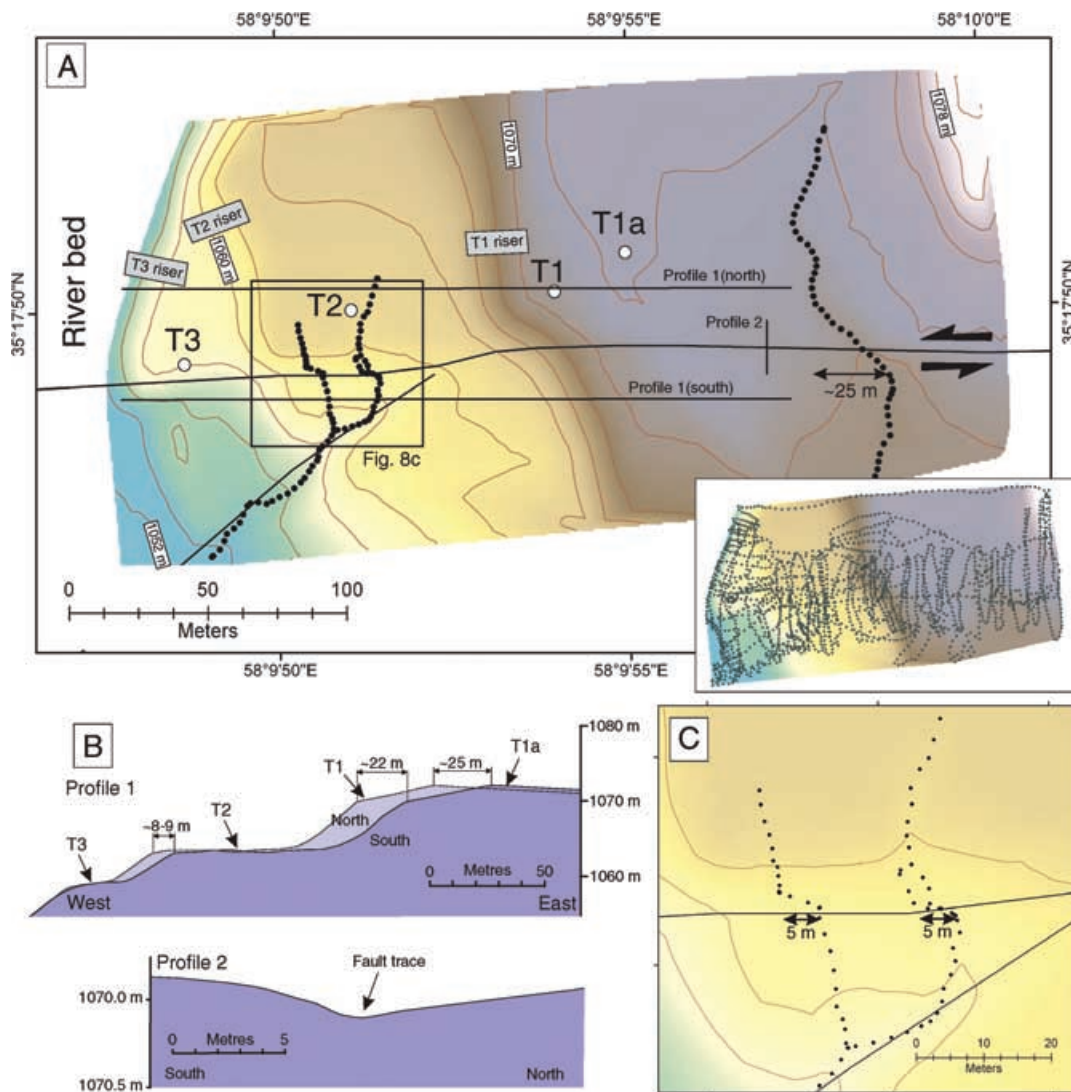


Figure 8. (a) A DEM (Digital elevation model) of the Doruneh fault at the eastern bank of the Shesh–Taraz river produced from differential GPS measurements. The DEM is contoured at 2 m intervals. The active river channel is at the left-hand side of the image. Three southward-flowing streams are marked as dotted black lines. The three main levels (T1, T2 and T3) are labelled. Risers between the levels are marked by grey rectangles. The highest level (T1a) appears to be a channel bank deposit (see Fig. 8b). A remnant of an older alluvial fan deposit is visible in the upper right corner. The four OSL sample locations are marked by white dots. The inset shows the GPS points used to construct the DEM. (b) Profiles through the Shesh–Taraz DEM, lines of section are marked on Fig. 8a. Profile 1 shows parallel east–west sections to the north and south of the fault. Left-lateral offset of each terrace riser, and the apex of the channel bank T1a, have been marked. Profile 2 is a north–south section across the fault showing the partially infilled ruptures seen in Fig. 9b. (c) Close-up view (see Fig. 8a for area) of two adjacent streams displaced left-laterally across the fault by 5 m. A field photograph of one of the stream displacements is shown in Fig. 10a.

sediment, or by cutting a large block of cemented sediment whose light-exposed edges can be trimmed in the laboratory. Our samples were collected from pits dug into the top surface of the terraces. Loose sediment was scraped into a bag whilst protected from the light by coverings of black plastic and canvas blankets. Our sampling strategy was adopted as the sediment was too coarse grained to enable the insertion of a tube and was not cohesive enough to allow cutting of a large block. We are confident that no light entered the pit whilst the samples were taken. Dose rates were measured in the lab by ICP-MS analysis of U, Th and ^{40}K concentrations in each sample. Further details of the methods, analytical techniques and results are provided in Appendix A. The luminescence of both quartz and feldspar grains were measured. However, the quartz grains were found to show a broad scatter in the measured equivalent dose between aliquots of each sample, with some failing to show any signal

at all, and it is likely that the age constraints obtained from the quartz grains will be unreliable though we do not know why the feldspar and quartz grains should show such different behaviours. In Table 2 we hence report the measured dose, dose rate and age estimates for the feldspar grains only. The reported errors are 1σ . The corresponding data from the quartz separates is provided for reference in Table A3. The feldspar analyses were performed for grain sizes between 90–180 (μm) and 180–250 (μm). An experimentally derived correction has been applied to account for anomalous fading of the luminescence signal of ~ 20 per cent in the feldspar grains. Further details of the experimental procedures and corrections applied are given in Appendix A.

The luminescence age determined for the T1 surface is 10.6 ± 1.3 ka. The T1a surface, which we assume from its morphology to be the same age as T1, has an age of 9.9 ± 4.6 ka. As described

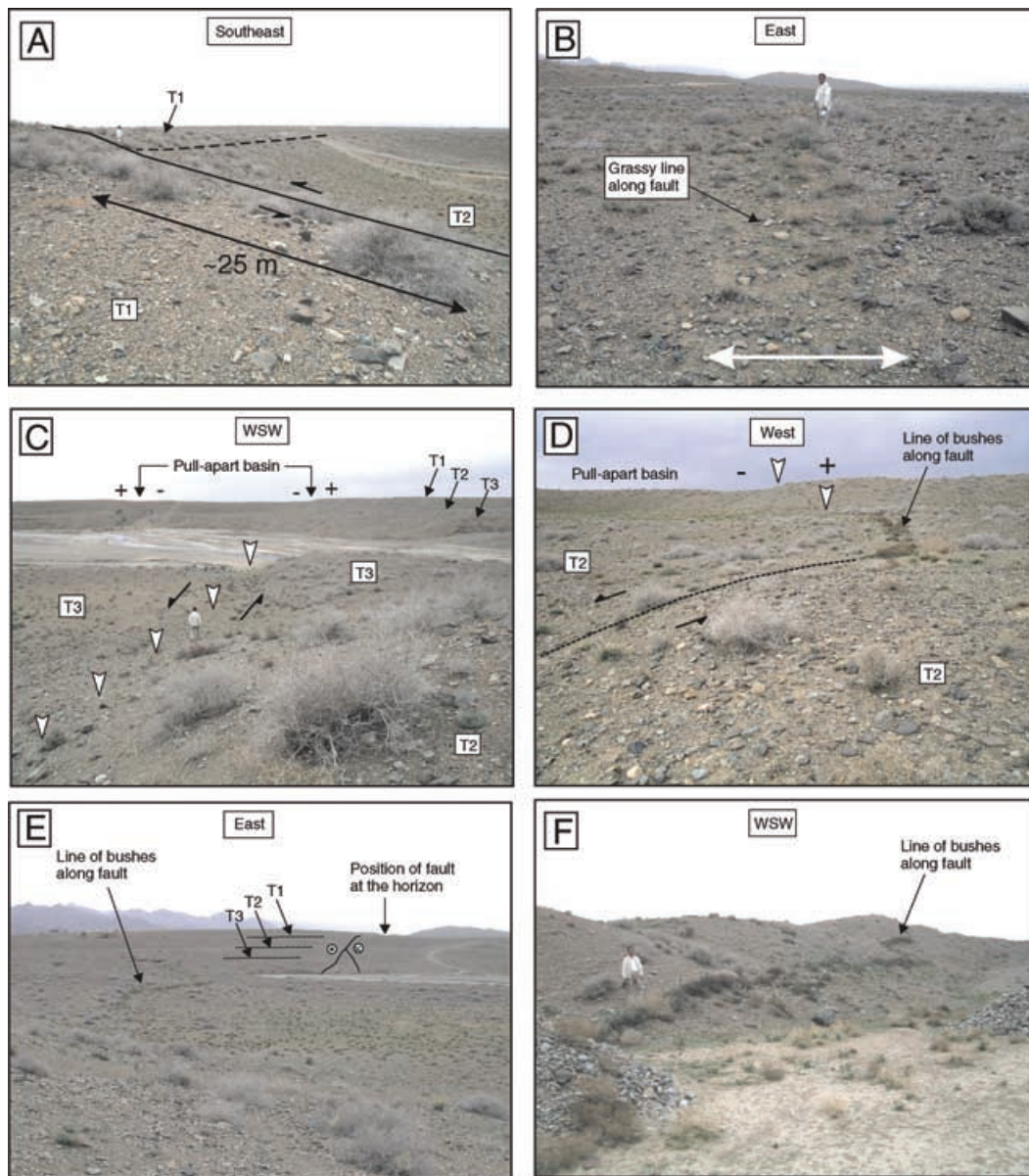


Figure 9. Field photos of the Doruneh fault at the Shesh–Taraz river. See Fig. 7c for locations. (a) View southeast from the top of the T1–T2 terrace riser on the northern side of the fault (at $35^{\circ}17'49.5''\text{N } 58^{\circ}09'55.3''\text{E}$). The top of the T1–T2 riser on the southern side of the fault is marked by a dotted line, and has been displaced ~ 25 m left-laterally. (b) View east of a shallow linear depression (~ 10 – 20 cm deep) along the Doruneh fault trace at $35^{\circ}17'49.5''\text{N } 58^{\circ}09'55.3''\text{E}$ (also see topographic profile in Fig. 8b). The ground surface within the depression is grassy, and scattered with a few pebbles, in contrast with the surrounding desert pavement (locally termed ‘Dasht’). (c) View looking WSW from $35^{\circ}17'49.3''\text{N } 58^{\circ}09'49.6''\text{E}$ from the top of the T2–T3 terrace riser on the northern side of the fault. The fault (marked by white arrows) cuts through the T3 terrace. The pull-apart basin, and the three terrace levels, can be seen at the far side of the Shesh–Taraz river. (d) View west from $35^{\circ}17'48.9''\text{N } 58^{\circ}09'41.8''\text{E}$ of ~ 1 m high fault scarp in the T2 surface on the western bank of the Shesh–Taraz river. The base of the scarp is marked by a line of bushes. The scarp in the T1 surface can be seen in the distance. (e) View looking east from $35^{\circ}17'46.8''\text{N } 58^{\circ}09'35.5''\text{E}$ at vegetation along the fault scarp. The three terraces are visible on the eastern bank of the river. Kuh-e Teagh Ahmad is visible on the horizon. (f) View looking WSW from $35^{\circ}17'44.4''\text{N } 58^{\circ}09'41.6''\text{E}$ at a line of vegetation along the southern fault branch in the pull-apart basin.

in Section 3.2, the ~ 25 m of offset in the T1a ridge is probably close to the true fault displacement since abandonment of the T1 surface. Using the age range of T1, the 25 m of displacement implies a slip-rate of $2.4 \pm 0.3 \text{ mm yr}^{-1}$. This is feasible, given the range of 2.5 – 10 mm yr^{-1} of left-lateral slip expected (see Section 2.1). The T1 surface is part of a large and widespread alluvial fan which has been fluvially incised (Fig. 7). The age of ~ 10 ka for deposition of the Shesh–Taraz fan correlates with a period of global climate change at the end of the last ice age. Other recent dating studies in Iran show a similar correlation, with incised fan surfaces at Sabzevar

to the north of the study area dated at 9–13 ka (Fattahi *et al.* 2006), and two generations of fans near Jiroft in southeast Iran dated at 5–9 ka and 13.6 ± 1.1 ka (Regard *et al.* 2005; REGARD *et al.* 2006). The transition from glacial conditions to a relatively wet climate at the end of the last ice age has been correlated with the formation of widespread fan deposits elsewhere in Asia (e.g. Poisson & Avouac 2004).

The luminescence samples from the two lower Shesh–Taraz terraces (T2 and T3) are 8.2 ± 2.8 ka and 7.9 ± 3.1 ka, which are slightly younger than the measured age of T1. As the measured ages of T2

Table 2. Values used to calculate luminescence ages for the six samples. The second age column shows an average of the results for the 90–180 and 180–250 μm grain size ranges. See the appendix for full details of the analytical procedures used to calculate the ages.

Sample ID	Grain size (μm)	De (Gyr)	Dose rate (Gyr/ka)	Age (ka)	Average Age (ka)
T1a	90–180	25.7 ± 4.6	2.8 ± 0.2	9.2 ± 1.8	9.9 ± 4.6
T1a	180–250	29.4 ± 11.8	2.8 ± 0.2	10.7 ± 4.3	–
T1	90–180	24.5 ± 2.8	2.3 ± 0.1	10.6 ± 1.3	10.6 ± 1.3
T2	180–250	21.9 ± 7.4	2.7 ± 0.1	8.2 ± 2.8	8.2 ± 2.8
T3	90–180	23.1 ± 9.0	2.9 ± 0.2	7.9 ± 3.1	7.9 ± 3.1
Kfan1	90–180	268.2 ± 48.4	4.4 ± 0.2	61.4 ± 11.5	48.0 ± 14.7
Kfan1	180–250	149.2 ± 38.2	4.3 ± 0.2	34.7 ± 9.1	–
Kfan2	90–180	274.5 ± 52.5	5.3 ± 0.2	51.4 ± 10.2	51.4 ± 10.2

and T3 are younger than those determined for T1 we would suggest that cutting of the two lower terraces is likely to have occurred after deposition of the T1 fan, although as the age ranges of all samples do overlap, we cannot be sure of this from our analyses alone. Pottery fragments of unknown age have been found within the T3 terrace (Giessner *et al.* 1984). The presence of pottery fragments supports the assertion that the lower terraces post-date the formation of T1. Although no age is given for these pottery fragments, their presence suggests that the true age of deposition lies at the younger end of the T3 age range.

The two OSL ages of 48.0 ± 14.7 ka and 51.4 ± 10.2 ka determined for the Uch Palang fan, which is offset left-laterally by ~ 800 – 850 m, give much larger slip-rate estimates of ~ 16 – 18 mm yr^{-1} . The estimates from Uch Palang appear far too high to be plausible considering that only a small fraction of the ~ 25 mm yr^{-1} of Arabia-Eurasia convergence is accommodated in northeast Iran (e.g. Vernant *et al.* 2004). The Kfan1 and Kfan2 samples were taken from separate sample pits, and the similarity of the measured ages suggests that we are seeing a real depositional effect. Presumably we have sampled younger deposits, potentially from some more recent outwash event, which have mantled the Uch Palang fan surface. However, we did not see any clear evidence in our two sample pits for such an event.

If we are correct in interpreting the Uch Palang samples as originating from an overlying mantle of younger material it opens the possibility that the alluvial fan and river terraces at the Shesh Taraz locality are also mantled by younger deposits. However, we are confident that this is not the case as (a) the Shesh Taraz locality preserves a very sharp offset in each river terrace riser (Later depositional events would be likely to blur these displacements), and (b) the measured age of 10 ka for the Shesh Taraz T1 fan surface correlates both with other young dated alluvial fans in Iran and with a period of global climate change at the end of the last ice age.

5 POTENTIAL FOR LARGE EARTHQUAKES ON THE DORUNEH FAULT

So far, we have described indications of long-term left-lateral slip on the Doruneh fault and then used the displacement of geomorphic features to estimate a left-lateral slip-rate of ~ 2.5 mm yr^{-1} . This rate should be treated as a minimum value, as the luminescence method might overestimate deposition ages in coarse-grained sediments such as those sampled in our study (see Section 4). However, the rate of slip alone does not help us to refine estimates of seismic hazard, as slip may occur as very occasional large earthquakes, regular smaller earthquakes, or even as continuous (or semi-continuous) aseismic slip. In this section, we describe field observations of poten-

tial ruptures from an earthquake of unknown age on the Doruneh fault that is preserved in the geomorphology. The ruptures, and stream displacements associated with them, allow us to determine the likely magnitude of slip generated during the last major earthquake on the central part of the fault.

The clearest indications of surface rupturing are found close to the Shesh–Taraz river (see Figs 7 and 8). The trace of the Doruneh fault on both the eastern and western margins of the river is remarkably clear. On the eastern side of the river, the fault cuts through the T1 surface as a shallow linear depression, ~ 1 m wide, and ~ 10 – 20 cm deep (see Figs 8b (profile 2) and 9b). The surface of the depression is grassed and scattered with occasional pebbles. This contrasts with the ground outside the depression, which is not vegetated, and has a well formed desert pavement of pebbles on its surface (e.g. Fig. 9b). We interpret the depression as a fissure which has been partially infilled with relatively fine-grained sediments derived from low-energy surface run-off and wind-blown deposition. We cannot be certain that the fissuring results solely from one earthquake event. However, the partially infilled fracturing is very reminiscent of palaeo-earthquake ruptures observed, for example, in Mongolia (e.g. Baljinyam *et al.* 1993; Walker *et al.* 2006).

As the fault cuts through the middle terrace (T2), it splits into two separate strands, which both acquire a vertical component of motion. Two small streams, which are incised into the T2 terrace surface on both sides of the fault, are deflected left-laterally by ~ 5 m at the northern fault strand (Fig. 8c, see also the photo in Fig. 10a). Further left-lateral offsets of the same amount (5 m) are observed along small incised streams on the western bank of the river (Fig. 10b and c). It is possible that the 5 m offsets arise from multiple repeated earthquakes. However, if this is the case, we might expect a scatter in the measured values of stream displacement. The similarity in displacement of each of these closely spaced streams, and the extremely sharp displacement of the streams across the fault trace, suggest to us that the offsets were formed during a single earthquake event with left-lateral slip of 5 m at this location. The sharp trace of the northern fault strand also cuts through the T3 surface, as seen in Fig. 9c.

On the western bank of the Shesh–Taraz river, the northern fault strand retains a very sharp vertical scarp, with a thin line of vegetation at its base (Figs 9d and e), and with further small incised streams displaced left-laterally at the scarp by ~ 5 m (two examples are shown in Figs 10b and c). The southern fault strand also has a very clear scarp, but the minor streams do not cross it, and are instead channeled eastward into the Shesh–Taraz river. There are hence no displaced markers to determine the magnitude of slip on the southern fault strand. The eastward-flowing diverted drainage has excavated a cutting on the northern (downthrown) side of the southern fault (Fig. 7c). A thin line of vegetation, several tens of

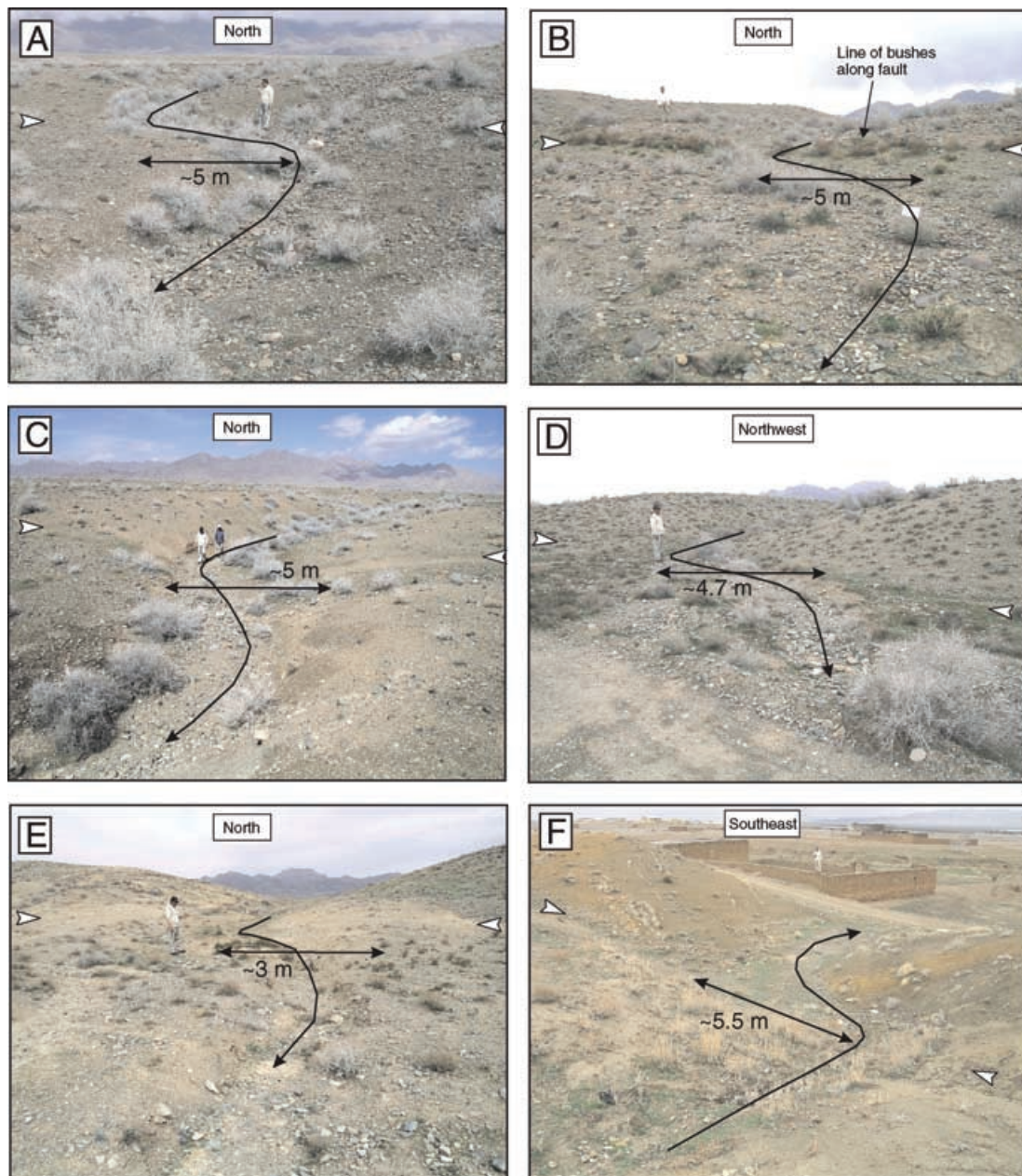


Figure 10. Field photos of stream displacements observed at the Doruneh fault. In each example, the stream channel is marked as a black line, and the fault scarp runs between white arrows. The magnitude of apparent left-lateral displacement was measured with a tape measure, and is likely to include uncertainty of at least ± 0.2 m. (a) 5 m stream displacement measured at $35^{\circ}17'48.6''\text{N } 58^{\circ}09'51.6''\text{E}$. (b) 4.5 m stream displacement measured at $35^{\circ}17'48.8''\text{N } 58^{\circ}09'43.7''\text{E}$. (c) 5 m stream displacement measured at $35^{\circ}17'46.0''\text{N } 58^{\circ}09'35.8''\text{E}$. (d) 4.7 m displacement $35^{\circ}17'49.7''\text{N } 58^{\circ}15'27.5''\text{E}$. (e) 3 m stream displacement measured at $35^{\circ}17'47.8''\text{N } 58^{\circ}15'43.5''\text{E}$. (f) 5.5 m displacement measured at $35^{\circ}17'13.2''\text{N } 58^{\circ}28'47.4''\text{E}$.

metres long, was found along the base of the scarp in this cutting (Fig. 9f). The line of vegetation is similar to those seen at the northern fault scarp, but as it is not associated with a clear scarp of tectonic origin we cannot be certain that the vegetation is running along a fault-related feature.

Left-lateral stream displacements are not only found on the Shesh–Taraz river terraces. A brief reconnaissance between the Shesh–Taraz river and the Uch Palang alluvial fan uncovered several other examples of minor streams which appear to have been displaced left-laterally by amounts varying from ~ 3 m to ~ 5.5 m (see Fig. 10d–f). The quality of the stream displacements varies between localities. Perhaps the best-preserved stream displacement is

shown in Fig. 10f, where the most recent fault trace cuts through a zone of fault gouge. A southward-flowing stream channel has a very clearly defined left-lateral displacement of ~ 5.5 m. We note that the majority of the minor streams crossing the Doruneh fault do not show a clear displacement. However, this is not a surprise, as it is only in those few examples where the stream is confined within an incised channel that clear evidence of the original course is likely to be preserved. The stream displacements vary from ~ 3 m to ~ 5.5 m, with a mean of ~ 4.7 m. Assuming that the displacements originated during a single earthquake event, as seems likely from the consistent 5 m stream offsets observed near the Shesh Taraz river, and the ratio of average slip to rupture length (\bar{u}/L) in the earthquake was

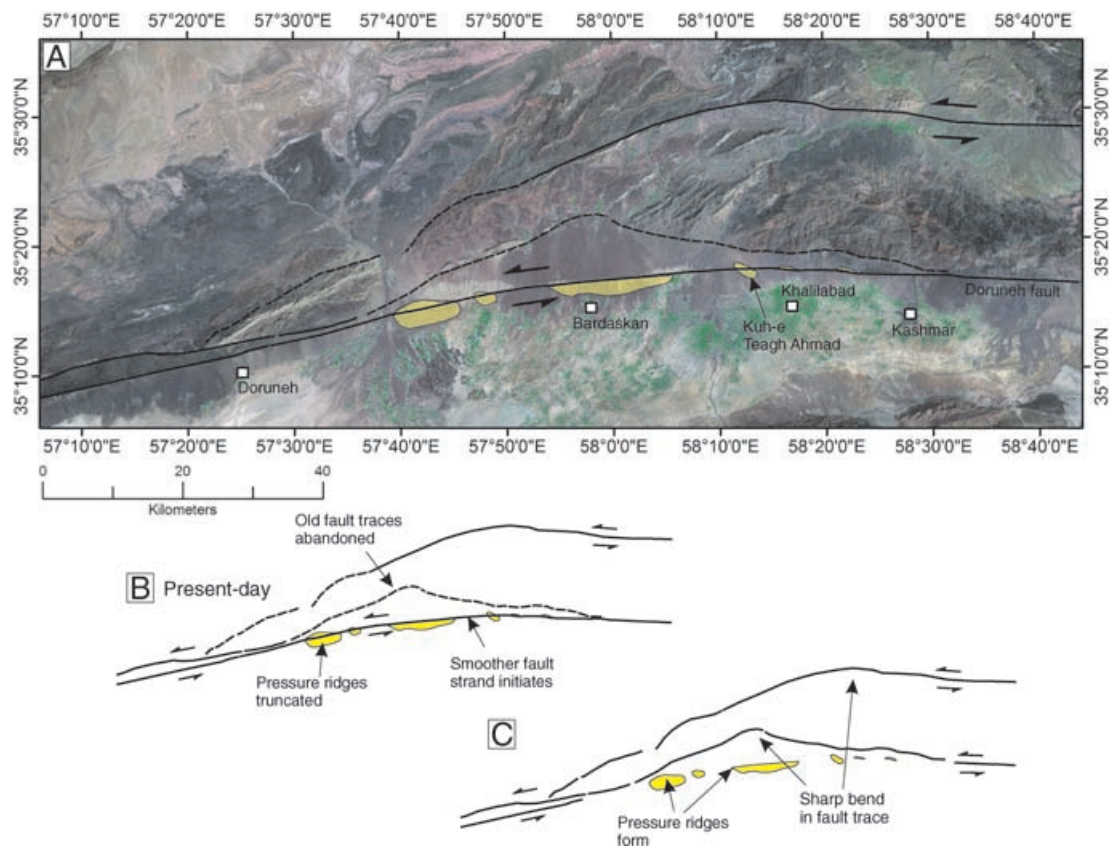


Figure 11. (a) MrSID LANDSAT TM+ mosaic (RGB 742) of the central section of the Doruneh fault (see Fig. 2 for location). Active faults are marked as solid lines. Faults inferred from sharp breaks in topography and from satellite imagery are marked as dotted lines. Short sections of these inferred geological faults are marked on the published geological map (Taheri & Shamasian 2001). All of the faults are marked on the map of Behzadi (1976). The two large strike-slip faults are marked on the map of Hessami *et al.* (2003). Small folds between Bardaskan and Kashmar (coloured in yellow) are cut through by the active trace of the Doruneh fault. (b) Sketch of the faulting shown in Fig. 11a. (c) Speculative interpretation of fault evolution in the area represented by Fig. 11a. The two older fault strands both bend sharply. Pressure ridges form in the alluvial cover south of the strike-slip faults as left-lateral shear starts to migrate away from the original fault strands. Eventually, the pressure ridges are abandoned as a new through-going strike-slip fault is formed. The new fault bypasses the sharp bend in the older fault traces.

5×10^{-5} , which is typical for continental earthquakes (Scholz 1982), the rupture length would have been ~ 100 km. A moment magnitude (M_w) of ~ 7.5 is calculated from the average displacement (4.7 m) following the empirical relationships of Wells & Coppersmith (1994).

We have no direct constraints on the age of the earthquake ruptures. Compared to many other regions of active tectonics, subtle indications of faulting in Iran are often very well preserved, due to the arid climate (e.g. Talebian & Jackson (2002); Walker *et al.* (2003); Hollingsworth *et al.* (2006)). Nonetheless, it is rare for surface ruptures from individual earthquakes to be preserved for considerable lengths of time (e.g. Ambraseys & Melville 1982), and the features observed along the Doruneh fault are exceptional. The earthquake ruptures are best preserved on the terraces of the Shesh–Taraz river at a small pull-apart in the fault trace. The site is uninhabited, and the pull-apart basin may have sheltered the landforms from erosion, thus prolonging the preservation of the scarps and ruptures. However, it is also possible that the earthquake happened relatively recently. Historical records in this part of Iran are not as comprehensive as in many other parts of Iran, as the Kashmar valley is isolated, and reliable records are often biased towards major trade routes (Ambraseys & Melville 1982). An upper limit on the age of the ruptures might be provided by the 18 m high 13th Century

minarets at Kishmar (Fig. 3) and Firuzabad (20 km southwest of Kishmar), see Ambraseys & Melville (1982) and Matheson (1972). Palaeoseismic trenching across the surface ruptures is needed to constrain the age of the last earthquake.

6 IMPLICATIONS FOR FAULT GROWTH AND EVOLUTION

This study has focused on determining the likely slip-rate of the Doruneh fault and its behaviour in earthquakes. However, our observations also have implications for how the fault has evolved through time. For example, the presently active, and throughgoing, strand of the Doruneh fault cuts through the core of the Kuh-e Teagh Ahmad fold and has displaced the eastern and western parts of the fold by at least 200–400 m (e.g. Fig. 6). Further east, however, the Uch Palang fan (which was dated at an implausibly young age of ~ 50 ka, see Section 4) is clearly displaced left-laterally by 800–850 m (Fig. 5). It therefore appears that the presently active fault trace initiated earlier in the east of the study area than in the west. At our estimated slip-rate of 2.4 ± 0.3 mm yr $^{-1}$ the strike-slip faulting at Kuh-e Teagh Ahmad might have initiated as little as 100 ka ago.

The Teagh Ahmad fold appears to have formed as a pressure ridge along a zone of east–west left-lateral shear. As this shear continued,

the fold has been abandoned and replaced by a through-going strike-slip fault. The Teagh Ahmad fold is only one of several short NW–SE aligned pressure ridges or folds, visible in digital topography, and spaced at ~5 km (e.g. Fig. 3b, see also Fig. 11). Though some of these other ridges are located at bends in the present fault trace, and are not abandoned like the Teagh Ahmad fold, they might also have formed in an early stage in the development of the fault (Fig. 11). It is likely that the 200–400 m of left-lateral slip on the presently active fault trace represents a migration of activity from one fault strand to another. An old, and presently inactive, fault is present along the base of Kuh-e Sorkh (Fig. 3b). This older fault trace can be traced westward from the longitude of Kashmar. East of Kashmar, where the larger magnitudes of slip are measured at Uch Palang, the old fault trace is still active.

The proposed fault evolution is shown in Fig. 11. The two pre-existing strike-slip faults (the Doruneh and Bijvard faults; Hessami *et al.* 2003) both bend sharply at longitude ~58° E (as noted by Behzadi 1976). It appears that the new fault strand near Bardaskan has formed in order to bypass the sharp bend in the faults. In our speculative models, aligned folds first formed in the alluvial cover near Bardaskan as left-lateral shear starts to migrate away from the original fault strands. Eventually, the folds are abandoned as a new through-going strike-slip fault is formed. We have no information at present on the total cumulative displacement along other parts of the fault.

7 CONCLUSIONS

The Doruneh fault is one of the major active structures in Iran and yet there are very few modern data on its structure and earthquake potential. Our results provide the first estimate of slip-rate on the fault and show that it is likely to have generated large magnitude (M_w 7–7.5) earthquakes in the past. The average 4.7 m left-lateral stream displacements, which we interpret as resulting from slip in this last earthquake event, would accumulate in ~2000 yr at the 2.4 ± 0.3 mm yr⁻¹ rate of slip determined in Section 4. Information on the age of the last earthquake, and a longer term record of earthquake events, would be revealed by palaeoseismic trenching across the surface ruptures.

ACKNOWLEDGMENTS

We thank the Geological Survey of Iran for their continued support of our work in Iran. RTW would especially like to thank M. Talebian for organizing the fieldwork logistics and M.R. Ghassemi for discussions on the Doruneh fault. Mr Arabi and Mr Califi were excellent drivers during this fieldwork. We thank N. Ambraseys for discussions on the earthquake history. The original version of this paper was improved by helpful reviews by V. Regard and R. Hetzel. The University of Birjand very kindly provided funding and logistical help during fieldwork in 2004 and 2005. The OSL analyses were performed as part of a grant awarded to RTW and MF by the Royal Society. This work was funded by NERC in the form of a research fellowship to RTW and through the Centre for the Observation and Modelling of Earthquakes and Tectonics (COMET). MF was supported by a research grant from the University of Tehran.

REFERENCES

- Adamiec, G. & Aitken, M., 1998. Dose rate conversion factors: update, *Ancient Thermoluminescence*, **16**, 37–49.
Aitken, M., 1985. *Thermoluminescence Dating*, Academic Press, London.

- Allen, M., Walker, R., Jackson, J., Blanc, E.-P., Talebian, M. & Ghassemi, M., 2006. Contrasting styles of convergence in the Arabia-Eurasia collision: Why escape tectonics does not occur in Iran, eds Dileky, Y. & Pavlides, S., *Geological Society of America Special Publication*, **409**, 579–589, doi:10.1130/2006.2409(26).
Ambraseys, N. & Melville, C., 1977. The seismicity of Kuhistan, Iran, *The Geographical Journal*, **143**, 179–199.
Ambraseys, N. & Melville, C., 1982. *A history of Persian earthquakes*, Cambridge University Press, Cambridge.
Ambraseys, N. & Moinfar, A., 1975. The seismicity of Iran; the Turshiz, Kashmar – Khorasan earthquake of 25th september 1903, *Annali de Geofisica*, **28**, 253–269.
Ambraseys, N. & Moinfar, A., 1977. The seismicity of Iran. The Kaj Darakht, Khurasan, earthquake of 25th May, 1923, *Annali de Geofisica*, **30**, 3–18.
Armitage, S. & Bailey, R., 2005. The measured dependence of laboratory beta dose rates on sample grain size., *Radiation Measurements*, **39**, 123–127.
Baker, C., 1993. Active seismicity and tectonics of Iran, *PhD thesis*, University of Cambridge.
Baljinnnyam, I. *et al.*, 1993. Ruptures of major earthquakes and active deformation in Mongolia and its surroundings, *Geological Society of America Memoir*, **181**, 62pp.
Behzadi, H., 1976. The tectonic history of east-central Iran, *PhD thesis*, University of Leeds.
Bell, W.T., 1980. Alpha dose attenuation in quartz grains for thermoluminescence dating., *Ancient TL*, **12**, 4–8.
Berberian, M. & Yeats, R., 1999. Patterns of historical earthquake rupture in the Iranian Plateau, *Bull. Seism. Soc. Am.*, **89**, 120–139.
Berberian, M. & Yeats, R., 2001. Contribution of archaeological data to studies of earthquake history in the Iranian Plateau, *Journal of Structural Geology*, **23**, 563–584.
Botter-Jensen, L., B., E., Duller, G.A.T. & Murray, A.S., 2000. Advances in luminescence instrument systems., *Radiation Measurements*, **32**, 523–528.
Engdahl, E., van der Hilst, R. & Buland, R., 1998. Global teleseismic earthquake relocation with improved travel times and procedures for depth determination, *Bull. Seism. Soc. Am.*, **88**(3), 722–743.
Fattahi, M. & Stokes, S., 2005. Dating unheated quartz using a single-aliquot regenerative-dose red thermoluminescence protocol, *Journal of Luminescence*, **115**, 19–31.
Fattahi, M. & Walker, R., 2006. Luminescence dating of the last earthquake on the Sabzevar thrust fault, NE Iran, *Quaternary Geochronology*, in press.
Fattahi, M., Walker, R., Hollingsworth, J., Bahroudi, A., Nazari, H., Talebian, S., Armitage, S. & Stokes, S., 2006. Holocene slip-rate on the Sabzevar thrust fault, NE Iran, determined using Optically-stimulated Luminescence (OSL), *Earth planet. Sci. Lett.*, **245**, 673–684.
Forman, S.L., Pierson, J. & Lepper, K., 2000. *Quaternary Geochronology*, chap. Luminescence Geochronology, pp. 157–176, American Geophysical Union.
Giessner, K., Hagedorn, H. & Sarvati, M., 1984. Geomorphological studies in the Kashmar region (NE Iran), *N. Jb. Geol. Palaont. Abh.*, **168**, 545–557.
Hessami, K., Jamali, F. & Tabassi, H., 2003. Map of Major Active Faults of Iran, Tech. rep., International Institute of Earthquake Engineering and Seismology, Iran.
Hollingsworth, J., Jackson, J., Walker, R., Gheitanchi, M. & Bolourchi, M., 2006. Strike-slip faulting, rotation, and along-strike elongation in the Kopeh Dagh mountains, NE Iran, *Geophys. J. Int.*, **166**, 1161–1177.
Jackson, J., 2001. Living with earthquakes: know your faults, *Journal of Earthquake Engineering*, **5**(Special Issue S1), 5–123.
Jackson, J. & McKenzie, D., 1984. Active tectonics of the Alpine-Himalayan Belt between western Turkey and Pakistan, *Geophys. J. R. astr. Soc.*, **77**(1), 185–264.
Jackson, J., Haines, J. & Holt, W., 1995. The accommodation of Arabia–Eurasia plate convergence in Iran, *J. geophys. Res.*, **100**(B8), 15 205–15 219.

- Matheson, S., 1972. *Persia: An Archaeological Guide*, Faber and Faber.
- McKenzie, D., 1972. Active tectonics of the Mediterranean region, *Geophys. J. R. astr. Soc.*, **30**, 109–185.
- Mejdahl, V., 1979. Thermoluminescence dating: beta-dose attenuation in quartz grains, *Archaeometry*, **21**, 61–72.
- Murray, A. & Wintle, A., 2000. Luminescence dating of quartz using an improved single-aliquot regenerative-dose protocol, *Radiation Measurements*, **32**, 57–73.
- Poisson, B. & Avouac, J.-P., 2004. Holocene hydrological changes inferred from alluvial stream entrenchment in North Tien Shan Northwest China, *The Journal of Geology*, **189**(4), 231–249.
- Prescott, J. & Hutton, J., 1988. Cosmic ray and gamma ray dosimetry for TL and ESR., *Nuclear Tracks and Radiation Measurements*, **14**, 223–227.
- Preusser, F., 2003. IRSL dating of K-rich feldspars using the SAR protocol: Comparison with independent age control, *Ancient TL*, **21**, 17–23.
- Regard, V. et al., 2005. Cumulative right-lateral fault slip across the Zagros-Makran transfer zone: role of the Minab-Zendan fault system in accommodating Arabia-Eurasia convergence in southeast Iran, *Geophys. J. Int.*, **162**, 177–203.
- Regard, V. et al., 2006. ^{10}Be dating of alluvial deposits from Southeastern Iran (the Hormuz Strait area), *Palaeogeography, Palaeoclimatology, Palaeoecology*, **242**, 36–53.
- Rhodes, E., 2000. Observations of thermal transfer OSL signals in glacial quartz, *Radiation Measurements*, **32**, 595–602.
- Scholz, C., 1982. Scaling laws for large earthquakes: consequences for physical models, *Bull. Seism. Soc. Am.*, **72**, 1–14.
- Stokes, S., Colls, A., Fattahi, M. & Rich, J., 2000. Investigations of the performance of quartz single aliquot DE determination procedures, *Radiation Measurements*, **32**, 585–594.
- Taheri, J. & Shamanian, G., 2001. 1:100,000 scale geological quadrangle map of Iran, kashmar sheet, *Geological Survey of Iran*, Tehran, Iran.
- Talebian, M. & Jackson, J., 2002. Offset on the Main Recent Fault of NW Iran and implications for the late Cenozoic tectonics of the Arabia-Eurasia collision zone., *Geophys. J. Int.*, **150**, 422–439.
- Tchalenko, J., Berberian, M. & Behzadi, H., 1973. Geomorphic and seismic evidence for recent activity on the Doruneh fault, Iran, *Tectonophysics*, **19**, 333–341.
- Van Der Woerd, J. et al., 2002. Uniform postglacial slip-rate along the central 600 km of the Kunlun fault (Tibet), from ^{26}Al , ^{10}Be and ^{14}C dating of riser offsets, and climatic origin of the regional morphology, *Geophys. J. Int.*, **148**, 356–388.
- Vernant, P. et al., 2004. Present-day crustal deformation and plate kinematics in the Middle East constrained by GPS measurements in Iran and northern Oman, *Geophys. J. Int.*, **157**, 381–398.
- Walker, R. & Jackson, J., 2004. Active tectonics and late Cenozoic strain distribution in central and eastern Iran, *Tectonics*, **23**, TC5010, doi:10.1029/2003TC001529.
- Walker, R. et al., 2006. Geomorphology and structure of the Jid right-lateral strike-slip fault in the Mongolian Altay mountains, *Journal of Structural Geology*, **28**, 1607–1622.
- Walker, R., Jackson, J. & Baker, C., 2003. Surface expression of thrust faulting in eastern Iran: source parameters and surface deformation of the 1978 Tabas and 1968 Ferdows earthquake sequences, *Geophys. J. Int.*, **152**, 749–765.
- Walker, R., Jackson, J. & Baker, C., 2004. Active faulting and seismicity of the Dasht-e-Bayaz region, eastern Iran, *Geophys. J. Int.*, **157**, 265–282.
- Wallinga, J., Murray, A., Duller, G. & Tornqvist, T., 2001. Testing optically stimulated luminescence dating of sand-sized quartz and feldspar., *Earth planet. Sci. Lett.*, **193**, 617–630.
- Wellman, H.W., 1966. Active wrench faults of Iran, Afghanistan, and Pakistan, *Geologische Rundschau*, **55**, 716–735.
- Wells, D. & Coppersmith, K., 1994. New empirical relationships among magnitude, rupture length, rupture width, rupture area, and surface displacement, *Bull. Seism. Soc. Am.*, **84**(4), 974–1002.

APPENDIX A: LUMINESCENCE DATING: PROCEDURES AND RESULTS

A1 Experimental procedure

For our analyses we have used Infrared stimulated luminescence (IRSL), which differs from Optically Stimulated Luminescence (OSL) in the use of infrared rather than visible light stimulation. The main application of IRSL is for dating using feldspar grains (e.g. Preusser 2003).

The samples were processed under subdued red light. A portion of the sample was wet-sieved to separate coarse grain quartz and feldspar (90–180 μm and 180–250 μm) size fractions and immersed for two days in 1 N HCl to remove carbonate, followed by two days immersion in H₂O₂ to remove organic material. Heavy minerals (density >2.72 g cm⁻³) were removed from the treated sample fraction (90–180 and 180–250 μm size fractions) by heavy liquid (sodium polytungstate) separations. A further heavy liquid separation (density = 2.58 g cm⁻³) separated quartz and potassium feldspar (density <2.58 g cm⁻³). The quartz was etched by 48 per cent HF for 50 minutes. At each stage of the separation procedures, samples were generously rinsed with distilled water. The quartz and feldspar separates were mounted as monolayers for the single aliquot analyses (approximately 5 mg per disc) on 10 mm diameter aluminum discs using a silicon spray as an adhesive.

All the experiments reported here were carried out using a Risø (Model TL/OSL-DA-15) automated TL/OSL system (fitted with a 90Sr/90Y beta source delivering $\sim 5 \text{ Gyr min}^{-1}$) equipped with an IR laser diode (= 830 nm) and a blue (= 470 nm) diode array ($p = 24 \text{ mW cm}^{-2}$) as stimulation sources. The intensity of light incident on the sample was about 400 mW cm⁻² Botter-Jensen et al. (2000). OSL was detected using a Electron Tubes bialkali PMT. Luminescence was measured through 7 mm Hoya U-340 filters.

A2 Single aliquot regenerative (SAR) protocol

Over the last few years the SAR protocol suggested by Murray & Wintle (2000) for quartz has been developed and used to measure equivalent doses (De) in both quartz and feldspar luminescence dating (e.g. Stokes et al. 2000; Wallinga et al. 2001; Fattahi & Stokes 2005; Fattahi & Walker 2006). The SAR procedure (Table A1) critically depends on the assumption that it is possible to measure a signal after each dose and stimulation cycle, which acts as a

Table A1. Generalized single aliquot regenerated sequence. Note that in steps 2 and 5, the sample has been heated to the pre-heat temperature using TL and held at that temperature for 10 s. In steps 3 and 6 OSL was measured following IRSL. The Observed L_x and T_x are derived from the initial IRSL signal (5 s) minus a background estimated from the last part of the stimulation curve. The corrected natural signal $N = L_0/T_0$, and the corrected regenerated signal $R_x = L_x/T_x$ (for $x = 1-5$).

Step	Treatment	Observed
1	Give dose	–
2	Pre-heat	–
3	Stimulation	L _x
4	Give test dose	–
5	Pre-heat	–
6	Stimulation	T _x
7	Return to step 1	–

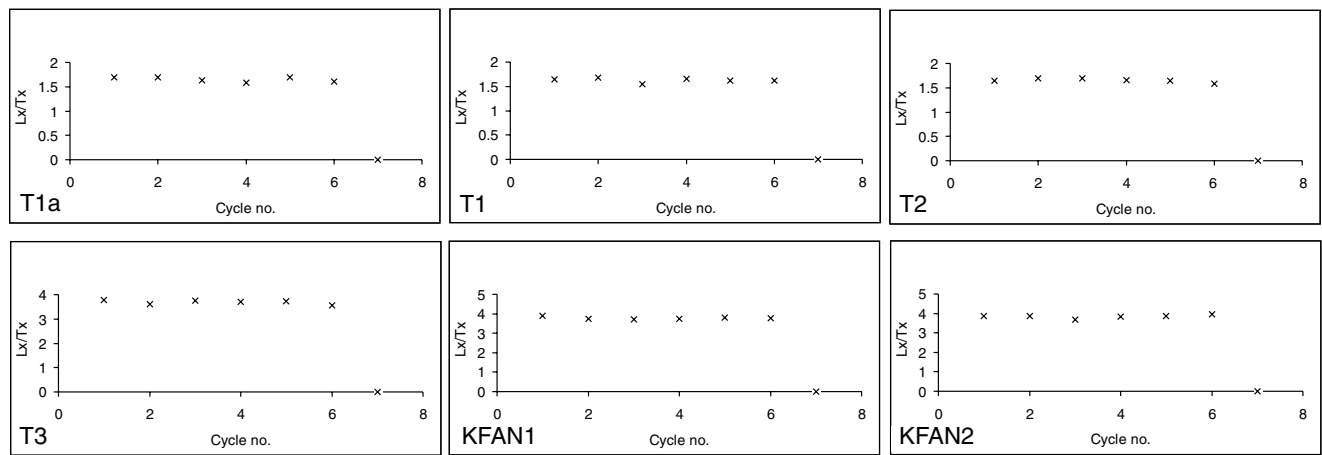


Figure A1. IRSL response to repeated fixed 16 Gyr regeneration (Lx), and 9.6 Gyr test (Tx) doses. The average sensitivity changes of three aliquots of each sample are determined by six repeated cycles in SAR.

surrogate measure of the sensitivity of the aliquot during the preceding measurement cycle. As such, any sensitivity changes which have occurred in the course of a regenerative analysis can be corrected for both the natural and regenerated signals.

Following the basic assumption of the SAR method, the equivalent dose (D_e) was obtained using this method for feldspar in the six samples collected from the Doruneh fault. Laboratory measurements of the beta dose rate were applied according to Armitage & Bailey (2005). The pre-heat and cut-heat treatment were similar. The pre-heat and cut heat used for all feldspar subsamples was either 260°C or 290°C for 10 s (unless otherwise stated) and the IRSL was measured for 200 s at a sample temperature of 125°C.

A3 Sensitivity changes and corrections

Sensitivity changes were checked by six repeated cycles of the SAR procedure with a repeated fixed regeneration and test dose. The fundamental assumption in the SAR protocol is that the sensitivity-correction procedure has worked properly if a plot of the regeneration dose IRSL (Lx) against the test dose IRSL (Tx) shows a straight line that passes through the origin (Murray & Wintle 2000). The above procedure was applied to check the validity of a test dose

to monitor and correct the sensitivity changes using three different heating methods. The regeneration dose was 16.0 Gyr and the test dose was 9.6 Gyr. All IRSL measurements were made for 200 s. The preheat temperature was 260°C for all measurements. Three aliquots were used for each measurement. Fig. A1 shows the average sensitivity changes of three separate aliquots for each sample. Although there is not a big sensitivity change for each sample the linear relationship passes through the origin (Fig. A2).

A4 Thermal transfer

To test for thermal transfer of charge into the IRSL trap as a result of preheating (e.g. Rhodes 2000) the natural aliquots were stimulated at room temperature, and the IRSL was measured for 200 s, with more than 4 hr delay between stimulation (to empty the rapid bleaching test). No significant IRSL signal was observed for the second measurement. This suggests that thermal transfer is not a likely source of uncertainty in these aliquots.

A5 Dose recovery tests

The aim of these experiments was to zero the IRSL signal using the same process as in the natural (unheated) portion. A known

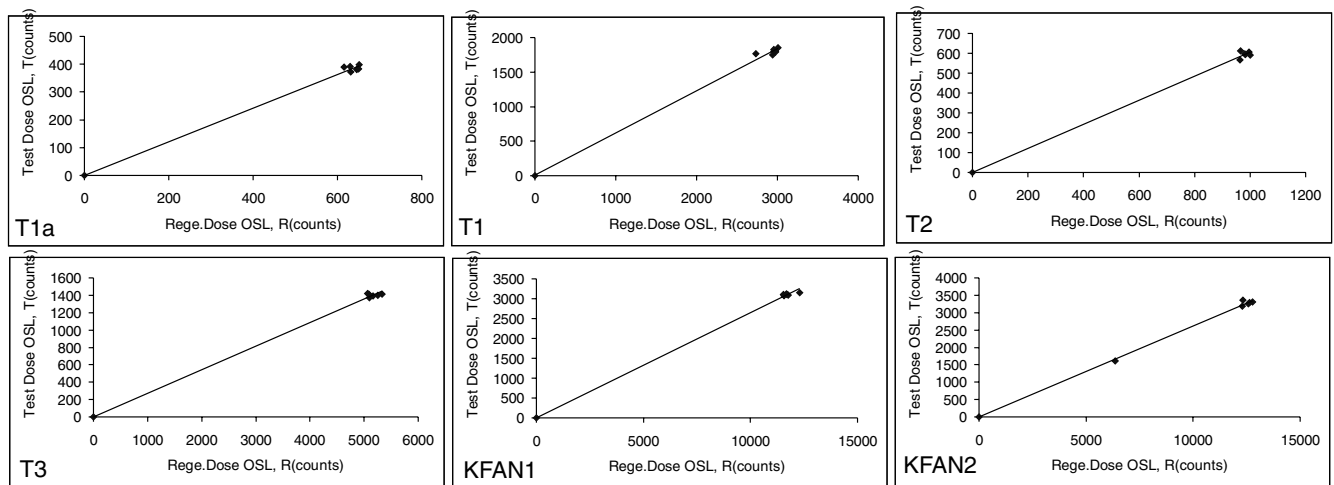


Figure A2. Repeated regeneration net IRSL signals (i.e., the first 5 s of measurement minus the average of the last 20 s) plotted versus the following net IRSL respond to the test dose.

laboratory dose, close to the expected natural dose, is given to the samples and the ability of SAR to accurately measure this dose is directly tested. Dose recovery tests also provide a method to determine whether the overall effects of sensitivity changes (which mainly occur after the sample is first heated) have been properly corrected for. However, as the dose rate is usually different in nature from the lab, only comparison with known age samples are able to test for any dose rate or time dependence effects. There are different approaches to zeroing the natural signal, of which we chose to stimulate the samples using infrared stimulation for 200 s at room temperature twice, with 10 hr room temperature storage between them. We expect this delay will allow the low temperature unstable TL traps to be emptied without heating the sample. Three aliquots were used for each pre-heat temperature. The pre-heat and cut heat temperatures were the same for each aliquot. After depleting the natural signal, following the above procedure, each aliquot was given beta doses close to the expected D_e (which for T1A, T1 and T3 is ~ 33 Gyr) and this dose was measured using the SAR procedures (Table A1) with the results shown in Fig. A3. The recycling ratios were all between 0.96 and 1.04. The recuperations are also shown in Fig. A3.

A6 D_e determination

According to our experiments, the quartz separates from the samples showed a dim signal and with scattered D_e distributions, and were therefore not very suitable for luminescence dating. The equivalent dose (D_e) for sample T1a (Fig. A4) was obtained using the single aliquot regeneration method (Table A1). The preheat time used for all measurements (250–290°C) was 10 s. IRSL was measured for 200 s at 1250°C sample temperature. Three disks were prepared for each preheat temperature and following measurement of the natural dose a dose–response curve was constructed from five dose points including three regenerative doses (~ 16 , 32 and 48 Gyr), and a zero dose. A replicate measurement of the lowest regenerative dose was carried out at the end of each SAR cycle. The net initial IRSL signal (the first 5 s minus the average of 180–200 s) was used for natural, regenerated and test dose measurements. The D_e was determined by interpolation and the sensitivity was corrected by dividing L_x by T_x . No aliquot produced significant recuperation signals (~ 2 per cent natural) and all produced a recycling ratio between 0.93 and 1.09. Fig. A4 shows a plateau in the pre-heat temperature range of 250 to 290°C for D_e values (mean $D_e = 21.43 \pm 3.86$ Gyr). We used this mean value for age determination. Based on this preheat plateau, we used either 260 or 290°C for 10 s as an appropriate temperature for equivalent dose determination of the other samples. Ten aliquots were prepared from each feldspar sample and following measurement of the natural dose, a dose–response curve was constructed from five dose points including three regenerative doses, and a zero dose (Fig. A5). A replicate measurement of the lowest regenerative dose was carried out at the end of each SAR cycle. Fig. A6 shows the dose distribution diagrams for all samples produced by Analyst software (G. Duller, 2005, personal communication).

A7 Anomalous fading test

A fading test was undertaken by performing ten repeated cycles of the SAR procedure with a fixed regeneration (~ 16 Gyr for T1, T1A, T2 and T3, and ~ 40 Gyr for Fan1 and Fan2) and test dose (~ 10 Gyr). After four cycles all aliquots were stored in the oven

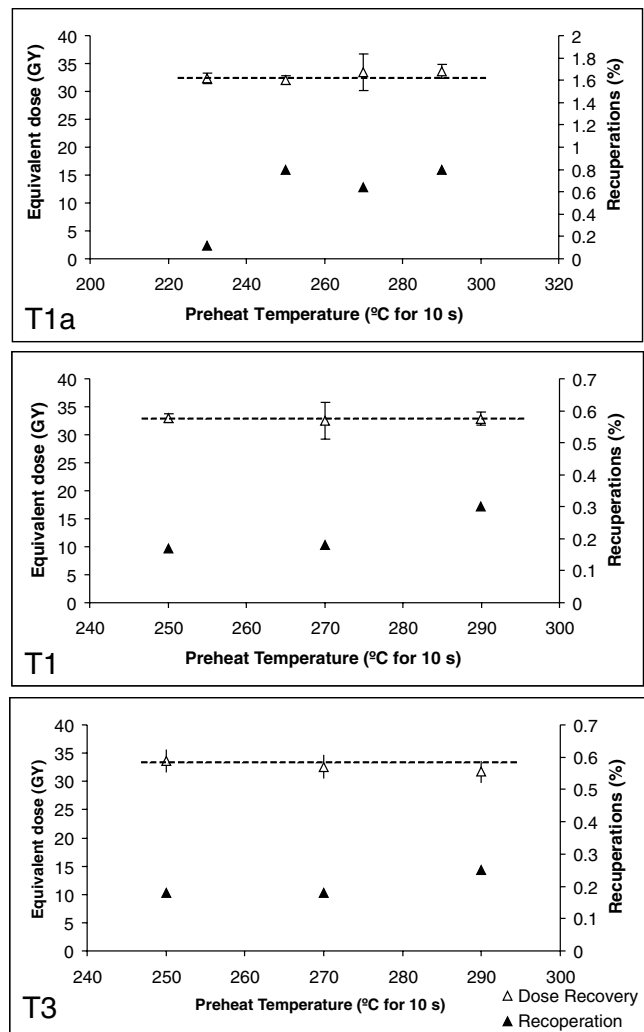


Figure A3. Dose recovery preheat plateau for samples T1, T1a and T3. After eroding the natural signal using two IRSL measurements at room temperature, with 10 hr room temperature storage between the measurements, a laboratory dose was given to the sample. This dose was then treated as a natural dose, and the D_e was determined using a range of regenerated doses from 16–48 Gyr and a test dose of 10 Gyr (see text for further details). The average D_e of three aliquots for each preheat temperature is plotted versus preheat temperature for 10 s.

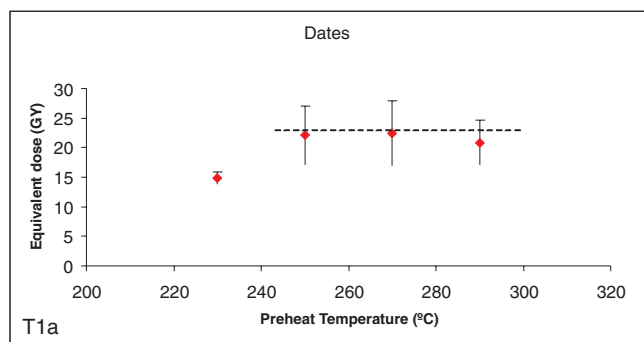


Figure A4. Plot of equivalent dose as a function of preheat temperature for sample T1a. The dashed lines are presented to show the accepted value of D_e (2.54 ± 0.08 Gyr) for age determination. The scattering of D_e measured for each preheat temperature is shown by a large variability in the error bars.

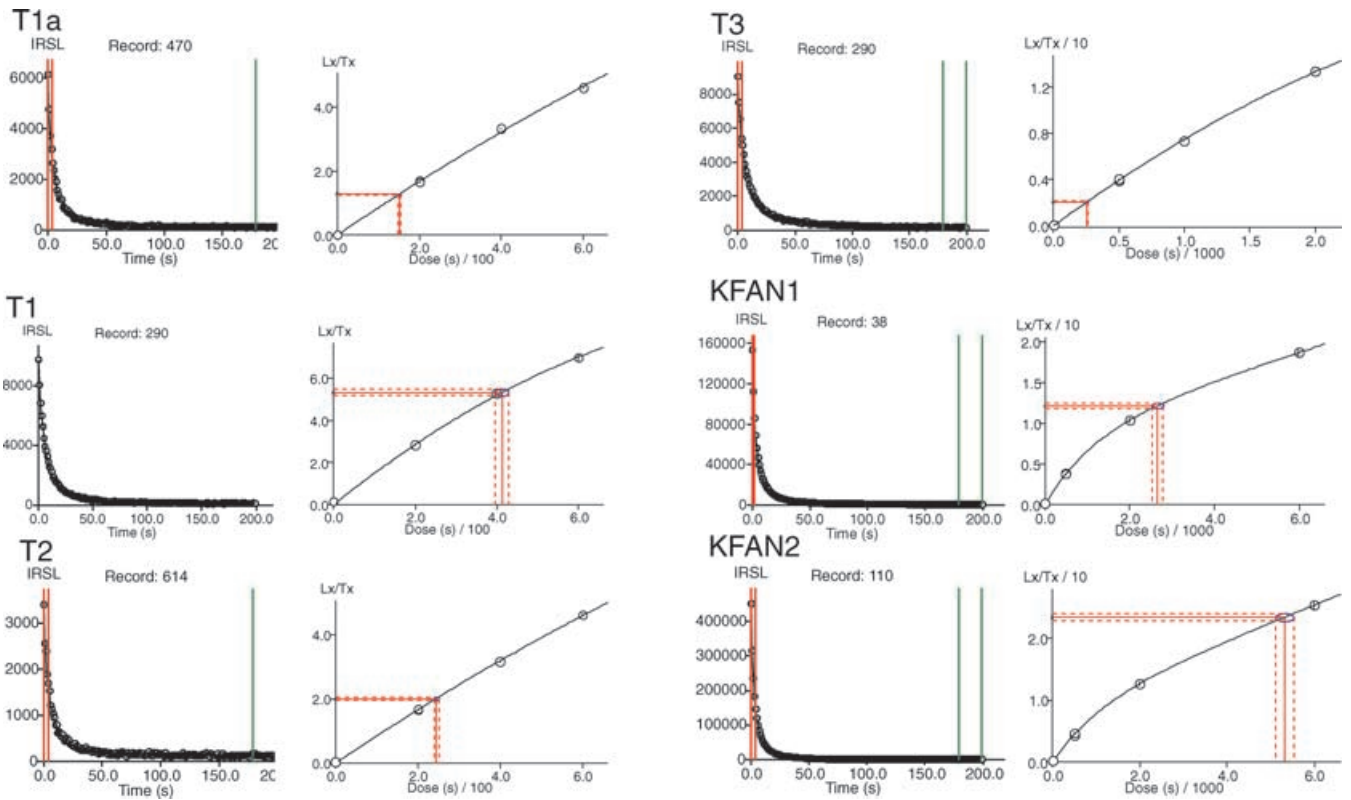


Figure A5. Examples of IRSL decay (left side), and dose response curves (right side), for all 6 samples. For De determination five regeneration doses (L_x , $x = 1, 2, 3, 4, 5$) are given. The sensitivity changes of regenerated IRSL data are then corrected by dividing by the subsequent IRSL test dose response (T_x , $x = 1, 2, 3, 4, 5$). The ratio (L_x/T_x , $x = 1, 2, 3, 4, 5$) is shown as open circles. A fit is applied to the regenerated data points. De is determined using net IRSL signals (i.e., the first 5 s of measurement minus the average of last 20 s), by interpolation (red lines).

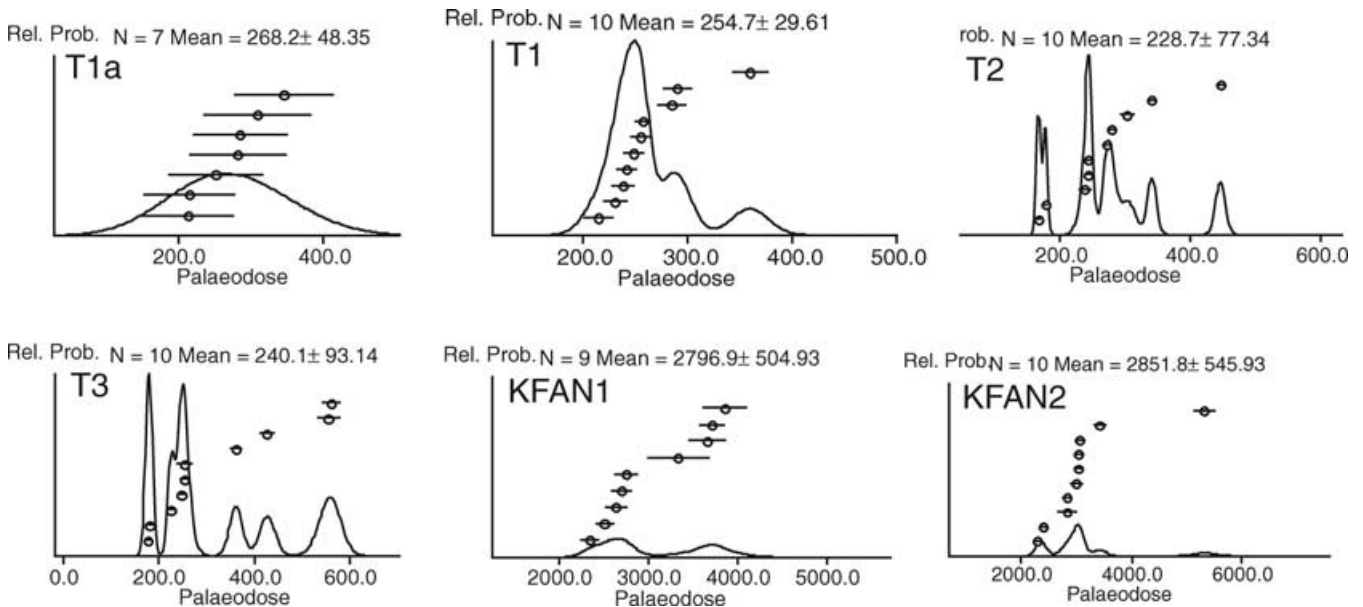


Figure A6. Equivalent dose distribution diagrams from SAR OSL for each of the feldspar samples. The equivalent dose distributions are displayed as probability density functions with individual aliquot De values superimposed in ranked order. N gives the number of individual aliquots for each sample. The units on the x-axis are seconds, and represent the number of seconds of exposure to a known beta source (in this case providing $\sim 5 \text{ Gyr min}^{-1}$) required to reproduce the natural luminescence signal. The diagrams provide a visual measure of the degree of resetting of the luminescence signal on deposition. If there is a close agreement between the measured equivalent dose for each aliquot of a sample the assumption of resetting is more likely to be valid. If there is significant scatter in the equivalent dose measurements it is likely that the sediment was not completely reset, and the mean age will overestimate the true deposition age. The well-defined peak in measured palaeodose for the T1 and T1a samples suggests that the measured ages are close to the true deposition ages.

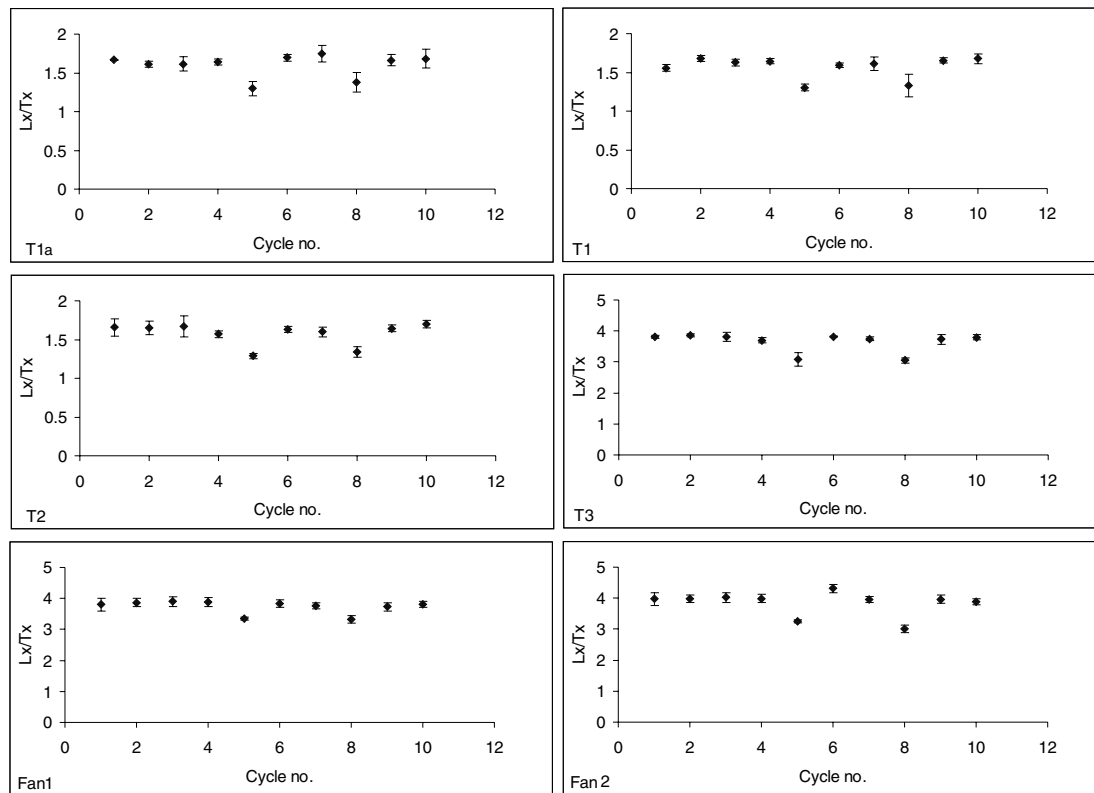


Figure A7. Fading test results. Sensitivity corrected IRSL signal as a function of repeated cycles using 260°C preheating temperature. The average of three aliquots is used for each cycle (see text for further details).

at 100°C following exposure to ~16 Gyr for T1, T1A, T2 and T3, and ~40 Gyr for Fan1 and Fan2. After 10 days storage at 100°C in the oven, the regeneration signal and response to the test dose (~10 Gyr) was measured (fifth cycle). Then, after two more cycles of the SAR procedure all aliquots were stored at room temperature, again following exposure to ~16 Gyr for T1, T1A, T2 and T3 and ~40 Gyr for Fan1 and Fan2. After 24 weeks, the regeneration signal and response to the test dose (~10 Gyr) was measured (8th cycle). Then, two more cycles of SAR with a similar fixed regeneration and test dose were repeated. The results are shown in Fig. A7. The average of these measurements for each sample shows a drop at cycle numbers 5 and 8. The fading ratio following storage in the oven was calculated by the ratio of the sensitivity corrected IRSL of the stored dose (L5/T5) divided by the average of the sensitivity corrected IRSL before storage (L4/T4) and the ratio of prompt measurement

after storage (L6/T6). Similar calculation was repeated for storage at room temperature and (L8/T8) divided by the average of (L7/T7) and (L9/T9). This suggests that the samples suffer from a maximum of ~20 per cent fading for the periods tested. Therefore, the measured D_e for all samples was corrected for 20 per cent fading.

A8 Dose rate and age determination

Dose-rates for each sample were calculated using radioisotope concentrations, burial depth and present-day moisture content. Uranium, thorium and potassium concentrations were measured using ICP mass spectrometry (Table A2). Present-day moisture contents were determined by drying at 40°C in the laboratory. Alpha, beta and gamma dose rates were calculated from radioisotope and

Table A2. Values used to calculate the total dose rate. Uncertainties are based on the propagation, in quadrature, of errors associated with individual errors for all measured quantities. In addition to uncertainties calculated from counting statistics, an error of 3 per cent is included due to beta source calibration (Armitage & Bailey 2005).

Sample	Grain size (μm)	Depth (m)	Water (per cent)	α -rate (Gyr/ka)	β -rate (Gyr/ka)	γ -rate (Gyr/ka)	Cosmic ray rate (Gyr/ka)	K (per cent)	U (ppm)	Th (ppm)	Total dose rate (Gyr/ka)
T1a	90–180	0.55	2 ± 2	0.03 ± 0.02	1.8 ± 0.08	0.76 ± 0.03	0.23 ± 0.13	1.43 ± 0.06	1.5 ± 0.08	5.4 ± 0.26	2.80 ± 0.16
T1a	180–250	0.55	2 ± 2	0.02 ± 0.01	1.8 ± 0.08	0.76 ± 0.03	0.23 ± 0.13	1.43 ± 0.06	1.5 ± 0.08	5.4 ± 0.26	2.76 ± 0.16
T1	90–180	0.4	2 ± 2	0.02 ± 0.01	1.5 ± 0.06	0.55 ± 0.03	0.25 ± 0.06	1.16 ± 0.05	1 ± 0.13	3.6 ± 0.41	2.31 ± 0.09
T2	180–250	0.4	2 ± 2	0.02 ± 0.01	1.7 ± 0.12	0.72 ± 0.03	0.23 ± 0.10	1.44 ± 0.05	1.3 ± 0.1	4.9 ± 0.21	2.68 ± 0.12
ta1	90–180	0.5	2 ± 2	0.03 ± 0.01	1.9 ± 0.08	0.76 ± 0.03	0.24 ± 0.13	1.64 ± 0.06	1.3 ± 0.08	5 ± 0.26	2.93 ± 0.16
Fan1	90–180	0.695	2 ± 2	0.04 ± 0.02	2.8 ± 0.12	1.25 ± 0.04	0.23 ± 0.13	2.70 ± 0.06	2 ± 0.08	8.3 ± 0.26	4.37 ± 0.19
Fan1	180–250	0.65	2 ± 2	0.03 ± 0.01	2.8 ± 0.12	1.25 ± 0.04	0.23 ± 0.13	2.70 ± 0.06	2 ± 0.08	8.3 ± 0.26	4.30 ± 0.18
Fan2	90–180	0.237	2 ± 2	0.05 ± 0.02	3.5 ± 0.16	1.5 ± 0.05	0.27 ± 0.13	3.54 ± 0.06	2.3 ± 0.08	9.1 ± 0.26	5.34 ± 0.21

water contents using the conversion factors of Adamiec & Aitken (1998) and Aitken (1985) respectively. Secular equilibrium in the uranium decay series was assumed. Alpha and beta dose rates were corrected for attenuation due to grain size using the factors of Bell (1980) and Mejdahl (1979). An alpha efficiency of 0.04 ± 0.02 was assumed for all samples. Cosmic ray dose rates were calculated from burial depth and overburden density (1.85 g cm^{-3}) using the formula given by Prescott & Hutton (1988). Potassium contents of 12.5 ± 0.5 per cent were used for the calculation of internal dose rate following Preusser (2003). Table A2 shows the values used to determine the annual dose ages. The derived age estimates are shown in Table 2.

A9 Discussion

The linear relationship between L_x and T_x passes through the origin (Fig. A2) and satisfies the basic requirement of the SAR method. The SAR IRSL showed a preheat plateau and recovered the known laboratory dose for each sample within their estimated error (Fig. A3). It also showed a preheat plateau for the natural D_e of sample T1a (Fig. A4). The SAR could successfully recover a given laboratory dose within 4 per cent on average. A plateau for D_e values of sample T1a in the pre-heat temperature range of 250 to 290°C, suggests that we can use this temperature range for D_e determination.

Preheating can result in thermal transfer from shallow traps to the traps sampled during OSL measurement. Unwanted thermal transfer can occur in nature if the light-insensitive traps are thermally unstable, and part of their charge is caught in OSL traps. Such thermal transfer can cause an overestimation of age and cannot be avoided by using a low preheat. However, significant thermal transfer was not observed for these samples. The result of fading tests showed that the feldspar grains are subject to anomalous fading of ~20 per cent, and as such, have provided an apparent deposition age which is younger than the real age. If we consider a natural fading of ~20 per cent then the D_e can increase by at least 20 per cent. The IRSL age of feldspar grains therefore indicates that the minimum age of these samples (assuming complete resetting) are as shown in Table 2.

A10 Quartz luminescence results

The luminescence of quartz grains were analysed as well as feldspar. The results are surprising in a number of ways. The dim signal and extremely large amount of scatter in the dose distribution diagrams for each sample suggests that the results are not reliable, and in the main text we have instead used the feldspar measurements. However, for completeness we include brief details of the quartz analyses below. The results are collated on Table A3. The Shesh–Taraz river terraces show an apparent increase in age from T1 to T3. From their stratigraphic positions, the opposite would be expected, with a decrease in age from T1 to T3, as is also shown in the feldspar IRSL results. That the T3 terrace is substantially younger than the 11.9 ka median age determined by Quartz luminescence is supported by the presence of pottery fragments (of unknown age) found within this terrace (Giessner *et al.* 1984).

The quartz luminescence gives an age of 5.9 ± 7.6 ka for the T1 surface. The T1a ridge, which we assume from its morphology to be the same age as T1, has a quartz luminescence age of 1.7 ± 1.3 ka. As described in Section 3.2, the ~25 m of offset in the T1 riser and T1a ridge is probably close to the true fault displacement since abandonment of the T1 surface. At the extreme maximum age for T1 of 3 ka, the 25 m of displacement implies a slip-rate of 8 mm yr^{-1} . This is feasible, given the range of 2.5–10 mm yr^{-1} of left-lateral slip expected (see Section 2.1). The two OSL ages of 21.9 ± 4.8 ka and 12.9 ± 2.9 ka determined for the Uch Palang fan, which is offset left-laterally by ~800–850 m, give a slip-rate estimate of 36–61 mm yr^{-1} .

Table A3. Equivalent dose, dose rates and calculated ages for Quartz grains (grain size range 90–180 μ) from the six samples.

Sample ID	Equivalent dose (Gyr)	Dose rate (Gyr/ka)	Age (ka)
T1a	3.8496 ± 2.9674	2.30 ± 0.17	1.7 ± 1.3
T1	10.7468 ± 13.7142	1.82 ± 0.16	5.9 ± 7.6
T2	6.1754 ± 8.5012	2.24 ± 0.17	2.8 ± 3.8
ta1	28.872 ± 15.639	2.42 ± 0.17	11.9 ± 6.5
Kfan1	83.408 ± 17.644	3.80 ± 0.20	21.9 ± 4.8
Kfan2	60.8718 ± 13.3934	4.71 ± 0.22	12.9 ± 2.9